Optimum Strategies for Monitoring the Operational Status of a Spacecraft

M. K. Simon, V. Vilnrotter, A. Mileant, and S. Hinedi
Communications and Systems Research Section

The design of a spacecraft-monitoring system based on a Neyman–Pearson detection criterion is discussed. Each noncatastrophic state of the spacecraft is indicated by the transmission of a specific signal to the ground station. Complete failure of the spacecraft is indicated by the transmission of no signal. The set of signals chosen to represent the spacecraft states consists of a group of orthogonally spaced (in frequency) carriers each with unknown (random) phase. Receiver structures derived from maximum-likelihood considerations are proposed that provide suitable performance in the presence of frequency uncertainty (due to Doppler) and frequency rate uncertainty (due to oscillator drift). Numerical results are obtained from a combination of analysis and simulation and indicate the trade-offs among the various receiver structures between performance and implementation complexity.

I. Introduction

The design of an optimum transmitter–receiver system for monitoring the operational status (state) of an orbiting spacecraft is best handled by applying the principles of maximum-likelihood detection used in hypothesis testing problems. In particular, each state of the spacecraft, e.g., spacecraft is fine, spacecraft has failed, spacecraft needs immediate attention, etc., is assigned a hypothesis and, based on an appropriately defined performance criterion, the receiver should be designed to minimize the power-to-noise ratio (or energy-to-noise ratio when fixing observation time) required to faithfully detect the hypothesis currently in effect. It is important to emphasize that the problem at issue here is one of *detection of a hypothesis* representing the state of a spacecraft (currently five states are being considered as representative of the operational scenario) as opposed to *detection of (decisions made on) data*, which is customarily associated with communication-type problems. While the two are indeed related in principle, e.g., for a binary data communication system, the polarity of each bit can be assigned to one of two hypotheses whereupon the data decision becomes a hypothesis testing problem, the measures used to define the fidelity of the two types of systems are quite different. At this point, it is of value to explore these differences in more detail.

In a data communication wherein one of $M(\geq 2)$ messages is to be communicated, the important measure of performance is average probability of error as a function of signal energy-to-noise ratio. In this scenario, wherein each message is represented by a signal to be transmitted over the channel, the signals are typically assigned equal energy, and more importantly, they are assumed to occur with equal a priori probability. Stated in terms of a hypothesis testing problem, each hypothesis to be tested by the receiver has equal a priori probability, namely, $1/M$, and this information is known to the receiver.

Furthermore, the costs associated with making decision errors are typically the same regardless of the type of error made. For example, in a binary communication system sending 0's and 1's message data, the decision that a "0" was sent when in reality a "1" was sent is equally as costly as deciding that a "1" was sent when in reality a "0" was sent. Because of this, the notion of cost usually does not enter into the performance criterion selected for characterizing a data communication system, i.e., the average error probability does not reflect the costs associated with each of the types of error committed.

By contrast, in a hypothesis testing problem of the type described above for monitoring and detecting the state of a spacecraft, the notion of cost is particularly appropriate. For example, the cost of an error in deciding that the spacecraft is fine when indeed it has failed is much larger than the cost of an error in deciding that it needs immediate help when indeed it might only need help at a later time. Also, the probabilities associated with the hypotheses that represent the various spacecraft states are, in general, quite unequal, e.g., the probability of complete spacecraft failure is significantly less than the probability that it might need some particular form of help. Furthermore, these a priori hypothesis probabilities might not be known to the receiver and, if they are, one can only estimate (approximate) their values from reliability studies performed on the spacecraft. Because of the above differences, it is readily apparent that a performance criterion such as minimizing the average probability of error (an optimum receiver would then be one that achieved this minimum average error probability with the smallest energy-to-noise ratio) is not appropriate to the spacecraft-state monitoring problem.

The next natural question to ask is: What is an appropriate performance criterion, and can it be formulated in terms of the principles of likelihood detection that are used as the basis of optimum data detection? The answer to this question can be partitioned into several possibilities depending on the amount of information made available to the receiver. If a reasonable set of a priori hypothesis probabilities is available and if an appropriate cost matrix (the ijth element of which is the cost associated with an error in deciding upon hypothesis H_j when in reality H_i is true) can be assigned, then the best criterion to apply is the so-called minimum risk or Bayes criterion, wherein one attempts to minimize the risk that is defined as the average (statistical) cost. This criterion is well documented for two hypotheses (states) and also documented but in less detail for more than two hypotheses. It is to be emphasized that in the situation where the a priori probabilities are all equal and the costs of all error types are equal (typically the costs associated with correct decisions are set equal to zero), then the Bayes criterion reduces to the maximum-likelihood criterion, which forms the basis of the minimum average-error probability criterion applied in data communication problems. Even if the a priori probabilities are not equal but the costs still are, then the Bayes criterion reduces to the maximum a posteriori (MAP) criterion, which still results in the minimization of average error probability.

In a less restrictive situation, where the cost matrix is known to the receiver but the a priori hypothesis probabilities are not, then a so-called min–max (or max–min) criterion can be applied, which is tantamount to minimizing the risk for a worst-case set of a priori probabilities, that is finding the maximum (over all choices of a priori probabilities) of the minimum risk found by applying the Bayes criterion. Depending on the relation between the actual a priori probabilities at issue and the worst-case set from the max–min criterion, such a design could conceivably be quite pessimistic. Nevertheless, it does provide a lower bound on the performance of the system, i.e., in the presence of the true a priori probabilities, the system will perform better than that predicted by application of the above worst-case set.

Finally, if both the a priori probabilities and the cost matrix are unknown to the receiver, then a so-called Neyman–Pearson criterion is often applied, in which one maximizes the probability of correct detection for a given probability of false alarm. More often than not, this criterion is used in the two-hypothesis case since there the notions of correct detection and false alarm are well defined in terms of the signal-present versus signal-absent concept. While it is possible to extend this criterion to more

than two hypotheses,[1] the literature completely avoids this discussion. The primary reason for this is as follows: While the notion of false alarm can still be meaningfully defined, i.e., deciding on any of the other hypotheses corresponding to a signal present when indeed a signal is absent (spacecraft is dead), the notion of correct detection is somewhat ambiguous since there are now many possible signal-present hypotheses to decide upon; hence, there are many correct detection probabilities—one associated with each of the signal-present hypotheses.

In summary, as far as the choice of a decision criterion is concerned, it is our belief that the minimum average-cost (Bayes) criterion is most appropriate to the problem at hand. Even though the a priori probability and cost information may not be exact, it is our belief that it is better to include it in the selection of a decision criterion (and thus a receiver architecture) rather than to ignore it entirely. It is clear, of course, that one will have to examine the sensitivity of such a design to the accuracy of the a priori probability and cost estimates supplied.

Regardless of which of the above criteria is selected, the optimum receiver structure that results will be independent of the correlation properties of the signals that represent the various spacecraft states. (Of course, the performance of the receiver will indeed depend on the signal correlation properties, and thus a second consideration in the design of an optimum system (transmitter–receiver) is to choose that signal set which optimizes the system performance for the given structure, determined from the decision criteria applied.) On the other hand, the specific implementation of the optimum receiver structure depends heavily on the amount of information known about the parameters that characterize the received signals, e.g., their phase, carrier frequency, etc. For example, if all signal parameters (e.g., carrier phase, frequency, etc.) are known, then the optimum receiver takes the form of some type of coherent receiver that may or may not include a priori probability and cost information, depending on the decision criterion adopted. At the other extreme, in the absence of any specific knowledge about the signal parameters, e.g., the carrier phase is assumed to be uniformly distributed in the interval $(-\pi, \pi)$, then the optimum receiver is a form of noncoherent receiver in that no attempt is made to estimate the carrier phase. While this may at first seem counter-intuitive, particularly to those whose minds are focused on the data communication problem, it must be understood that here the estimate of the phase must be performed over the same interval of time (or a shorter time dictated by signal dynamics) over which the signal must be detected, namely, the observation interval, whereas in the data communication case, the phase estimation time (which is related to the reciprocal of the bandwidth of, say, a carrier tracking loop) is large when compared to the signal-detection observation time interval, i.e., the bit interval. That is, the phase estimate is determined from an observation interval much longer than that used in making the data decision. One interesting, but strictly coincidental, situation occurs for the special case when the only unknown signal parameter is carrier phase. Here the noncoherent receiver and "pseudocoherent" receiver (i.e., obtain the maximum-likelihood phase estimate and then use that to perform "coherent" data detection) yield identical performance [1]. In all other instances, e.g., when, in addition, carrier frequency is uncertain due to Doppler, phase instabilities, etc., the pseudocoherent approach (based on first finding the best estimates of the unknown parameters and then using these in the detection process) is *inferior* (achieves a smaller detection probability for a fixed false alarm probability) to the noncoherent approach, wherein the parameters are assumed completely unknown. A caveat should be made here in that the above discussion assumes that *all unknown parameters are constant over the observation time interval*. When this assumption is violated, as would be the case in a realistic scenario, then neither the noncoherent nor the pseudocoherent approach is optimum any longer and it is possible that, under these circumstances, in the presence of some particular parameter variation scenarios, the latter might outperform the former. Such a conclusion will not result, however, from analysis (the model becomes too complex) but will ultimately have to be determined from a complete simulation of the system that takes into account the actual parameter variations that characterize the system. Finally, a compromise between

[1] In the spacecraft-monitoring problem, one of the hypotheses (corresponding to complete spacecraft failure) still corresponds to signal absent; however, the presence of several different spacecraft states necessitates several different signal-present hypotheses, each characterized by its own unique signal.

totally known and totally unknown parameter information, e.g., the carrier phase is characterized by a known probability density function, yields a form of partially coherent receiver.

It is important to stress here that application of the likelihood function principles to the problem at hand does not suggest any other form of receiver, such as coherent binary phase-shift keying (BPSK) or differential phase-shift keying (DPSK). While one can indeed propose a solution to the spacecraft-monitoring problem by specifying each signal in the form of a binary waveform and then applying the notion of differential detection (together with differential encoding at the transmitter) to design a receiver, such a proposal is an ad hoc solution to the problem at hand since differential detection is only optimum in the context of a data communication problem (minimize average-error probability) with an observation of two-bit intervals during which the carrier phase is assumed to be constant and unknown.

We begin the technical discussion of the article with a consideration of the Neyman–Pearson criterion as applied to multiple (more than two) hypothesis testing. The resulting test shall then form the basis of several receiver structures that are suggested as possible solutions to the spacecraft-monitoring problem when indeed the a priori state probabilities are assumed to be unknown.

II. A Neyman–Pearson Test for *M* Hypotheses

Consider a multiple hypothesis test in which the received signal $r(t)$ is characterized as follows:

$$r(t) = \begin{cases} n(t); & H_0 \\ s_i(t) + n(t); & H_i, i = 1, 2, \ldots, M-1 \end{cases} \tag{1}$$

where $n(t)$ denotes the additive channel Gaussian noise and $s_i(t),\ i = 1, 2, \ldots, M-1$ denotes the signals assigned to the noncatastrophic (other than complete failure) spacecraft states. Assuming that the noise-only condition (null hypothesis H_0) is indeed true, then deciding in favor of $s_i(t) + n(t)$ (hypothesis $H_i,\ i = 1, 2, \ldots, M-1$) results in a false alarm. Since all of these false alarm conditions come about from the same conditional hypothesis (namely, H_0), it is logical to define the false alarm probability P_{FA} by

$$P_{FA} = \sum_{i=1}^{M-1} \Pr\{ H_i | H_0 \} \tag{2}$$

Characterizing $r(t)$ in terms of a vector observable $\mathbf{r}$ corresponding to the coefficients in its Karhunen–Loeve expansion (a special case of which could be the sampling expansion) and denoting by R_i, $i = 0, 1, \ldots, M-1$ the set of disjoint regions in $\mathbf{r}$-space corresponding to choosing in favor of H_i, $i = 1, 2, \ldots, M-1$, then Eq. (2) can be expressed as

$$P_{FA} = \sum_{i=1}^{M-1} \int_{R_i} p(\mathbf{r} | H_0)\, d\mathbf{r} = 1 - \int_{R_0} p(\mathbf{r} | H_0)\, d\mathbf{r} \tag{3}$$

where $p(\mathbf{r} | H_0)$ is the conditional probability density function (pdf) of the vector observable $\mathbf{r}$ given the null hypothesis H_0.

Assuming that H_i is indeed true, then deciding in favor of $s_i(t) + n(t)$ results in a correct decision. We denote the probability of this event by

$$P_{Di} = \Pr\{H_i | H_i\} = \int_{R_i} p(\mathbf{r} | H_i)\, d\mathbf{r}, \quad i = 1, 2, \ldots, M-1 \tag{4}$$

In a two-hypothesis problem, i.e., $M = 2$, where there is only one correct detection probability, namely, $P_{D1} = \Pr\{H_1 | H_1\} \triangleq P_D$, the Neyman–Pearson test is derived from the criterion of maximizing P_D subject to a constraint on P_{FA}. Note that this is meaningful and can be achieved independently of the knowledge of the a priori probabilities of H_0 and H_1. While in the M hypothesis problem it is still meaningful to constrain false alarm probability, the presence of a set of $M-1$ correct detection probabilities, as in Eq. (4), presents many possibilities for the maximization part of the criterion. What one truly would like to do in the M-hypothesis case is to maximize the *average* correct detection probability (or, equivalently, to minimize the average missed detection probability) subject to a constraint on P_{FA}. In order to accomplish this, one needs knowledge of the a priori probabilities of the $M-1$ signal hypotheses (to allow computation of the average correct detection probability), which is contrary to the basic tenet of the Neyman–Pearson philosophy, namely, to specify a test that is independent of this knowledge. To arrive at a test that is simple and implementable, we shall choose to maximize the sum of the correct detection probabilities of Eq. (4), which is tantamount to maximizing the average correct detection probability *assuming equal a priori probabilities for the $M-1$ signal hypotheses*. Then, setting $M = 2$ will result in the well-known two-hypothesis Neyman–Pearson test, as mentioned above.

The above criterion can be formulated mathematically using the concept of LaGrange multipliers. For notational simplicity, let $p_i(\mathbf{r}) = p\{\mathbf{r}|H_i\}$, $i = 0, 1, 2, \ldots, M-1$. Then, the Neyman–Pearson test becomes the following: Choose the M decision regions R_i, $i = 0, 1, 2, \ldots, M-1$ so as to minimize

$$F = 1 - \sum_{i=1}^{M-1} P_{Di} + \lambda P_{FA} = 1 - \sum_{i=1}^{M-1} \int_{R_i} p_i(\mathbf{r}) d\mathbf{r} + \lambda \sum_{i=1}^{M-1} \int_{R_i} p_0(\mathbf{r}) d\mathbf{r}$$

$$= 1 - \sum_{i=1}^{M-1} \int_{R_i} \left(p_i(\mathbf{r}) - \lambda p_0(\mathbf{r})\right) d\mathbf{r} \tag{5}$$

where λ is a LaGrange multiplier to be determined. Thus, for a given observation $\mathbf{r}$, we examine all the values of i for which $p_i(\mathbf{r}) - \lambda p_0(\mathbf{r}) > 0$ and then choose that value of i, say i^*, which yields the *largest* of these positive values of $p_i(\mathbf{r}) - \lambda p_0(\mathbf{r})$. Then, $\mathbf{r}$ is assigned to the decision region R_{i^*}, i.e., based on observation of $\mathbf{r}$, we decide in favor of hypothesis H_{i^*}. Since the decision regions are disjoint, then for any particular value of $\mathbf{r}$, the contribution to the integral $\int_{R_i} \left(p_i(\mathbf{r}) - \lambda p_0(\mathbf{r})\right) d\mathbf{r}$ comes only from one of the terms in the summation on i, namely i^*. In terms of a likelihood ratio test, the above can be stated as

$$\left.\begin{array}{l} \text{If } \dfrac{p_i(\mathbf{r})}{p_0(\mathbf{r})} > \lambda, \text{ then choose hypothesis } H_{i^*} \text{ corresponding to } i^* = \max_i{}^{-1} \dfrac{p_i(\mathbf{r})}{p_0(\mathbf{r})}. \\ \\ \text{Otherwise (i.e., if } \dfrac{p_i(\mathbf{r})}{p_0(\mathbf{r})} \leq \lambda \text{ for all } i = 1, 2, \ldots, M-1), \text{ choose the hypothesis } H_0. \end{array}\right\} \tag{6}$$

In Decision Rule (6), the notation "$\max_i{}^{-1} f(i)$" means "the value of i that maximizes $f(i)$." The LaGrange multiplier λ (which from the above test turns out to be the decision threshold) is chosen to satisfy the given constraint on false alarm probability, which can be determined from

$$P_{FA} = 1 - \int_{R_0} p_0(\mathbf{r}) d\mathbf{r} \tag{7}$$

where $p_0(\mathbf{r})$ is independent of any of the transmitted signals, $s_i(t), \ldots, i = 1, 2, \ldots, M-1$. Note that Decision Rule (6) not only distinguishes between signal absent and signal present, but also decides on the most likely signal when indeed the latter is true. Returning now to the continuous time notation as originally introduced in Eq. (1) and also used throughout [1], Decision Rule (6) becomes

$$\left.\begin{array}{l} \text{If } \dfrac{p\left(r(t)\,|H_i\right)}{p\left(r(t)\,|H_0\right)} > \lambda, \text{ then choose } H_{i^*} \text{ corresponding to } i^* = \max_i{}^{-1} \dfrac{p\left(r(t)\,|H_i\right)}{p\left(r(t)\,|H_0\right)}. \\ \\ \text{If } \dfrac{p\left(r(t)\,|H_i\right)}{p\left(r(t)\,|H_0\right)} \leq \lambda \text{ for all } i = 1, 2, \ldots, M-1, \text{ choose } H_0. \end{array}\right\} \tag{8}$$

For the two-hypothesis case ($M = 2$), Decision Rule (8) simplifies to

$$\left.\begin{array}{l} \text{If } \Lambda\left(r(t)\right) \triangleq \dfrac{p\left(r(t)\,|H_1\right)}{p\left(r(t)\,|H_0\right)} > \lambda, \text{ then choose } H_1; \\ \\ \text{If } \Lambda\left(r(t)\right) \leq \lambda, \text{ then choose } H_0, \end{array}\right\} \tag{9}$$

where $\Lambda\left(r(t)\right)$ is referred to as the likelihood ratio.

III. Average- and Maximum-Likelihood Receivers Based on the *M*-Hypothesis Neyman–Pearson Test

In [1], average- and maximum-likelihood receivers were derived and presented for a variety of scenarios corresponding to the amount of parameter information, e.g., carrier phase, carrier frequency, etc., available for the signal. In all cases, the results were obtained only for the two-hypothesis case and as such related to the test for the presence or absence of a single signal. As discussed in the introduction, the spacecraft-monitoring problem corresponds to an M-hypothesis (typically a four-signal and one-null hypothesis, or $M = 5$) test, and thus it is of interest to reexamine the structure and performance of the receivers in [1] in light of the additional signal hypotheses.

As discussed in [1], the evaluation of the numerator of the likelihood ratio $\Lambda\left(r(t)\right)$ for a signal with unknown parameters requires that one first determine the pdf of the received signal under hypothesis H_1, conditioned on the vector of unknown parameters, and then average over the joint pdf of these parameters. Letting $\boldsymbol{\alpha}$ denote this random parameter vector (which, as mentioned above, would typically include carrier phase, carrier frequency, and possibly other frequency derivatives), then the likelihood ratio is computed from

$$\Lambda\left(r(t)\right) = \frac{\int_a p\left(r(t)\,|H_1\,, \boldsymbol{\alpha}\right) p(\boldsymbol{\alpha}) d\boldsymbol{\alpha}}{p\left(r(t)\,|H_0\right)} \tag{10}$$

This is referred to as the average-likelihood ratio (ALR) approach and is optimum in the context of the Neyman–Pearson criterion previously discussed. Ordinarily, the unknown random parameters are independent random variables, and thus the joint pdf $p(\boldsymbol{\alpha})$ becomes a product of the individual pdf's characterizing each parameter; hence, the multidimensional integral in Eq. (10) becomes a product of integrals.

An alternate approach is to compute the numerator of the likelihood function by again first determining the pdf of the received signal under hypothesis H_1 conditioned on the vector of unknown parameters,

but by then replacing the random parameters with suitable estimates of these parameters rather than averaging over their joint pdf. One such set of estimates is the maximum-likelihood (ML) estimates and leads to the maximum-likelihood ratio (MLR) approach, which is mathematically characterized by

$$\hat{\Lambda}\left(r(t)\right) = \frac{p\left(r(t)\,|H_1, \hat{\boldsymbol{\alpha}}_{ML}\right)}{p\left(r(t)\,|H_0\right)} \tag{11}$$

where $\hat{\boldsymbol{\alpha}}_{ML}$ is the ML estimate of the parameter vector $\boldsymbol{\alpha}$. Note that under no circumstances is $\hat{\Lambda}\left(r(t)\right)$ ever equal to $\Lambda\left(r(t)\right)$ and, except in some very specialized cases, the ALR and the MLR philosophies do not result in the same likelihood-ratio (LR) test. One case where they do result in the same LR test (as pointed out in [1]) occurs for a signal that is an unmodulated sinusoidal tone (carrier), all of whose parameters are known except for its phase, which is assumed to be uniformly distributed in the interval $(-\pi, \pi)$.

In a more general context, structures derived from replacing the unknown parameters in the pdf of the received signal under hypothesis H_1 conditioned on the vector of unknown parameters with estimates of them are referred to as estimator–correlator structures. The reason for this is that the form of these structures involves a correlation of the received signal plus noise, $r(t)$, with a suitable estimate of the transmitted signal followed by comparison with a threshold determined from the specified false alarm probability. In fact, it was shown almost three decades ago by Kailath [2] that receiver structures derived from an ALR test *always* have an equivalent formulation (leading to an equivalent likelihood ratio test) in terms of an estimator–correlator structure, provided that the appropriate signal estimator is used.[2] In this context, it was shown that the correct signal estimator to use in the estimator–correlator structure is the minimum mean-square estimator (MMSE) based on observation of the received signal up to the present time. Since the MMSE estimator of the signal up to the present time is not equal to the signal estimate obtained using ML estimates of the signal parameters obtained from the full observation interval, it is unlikely that the two will yield equivalent-likelihood ratio tests. Equivalently, the ALR (which is equivalent to the estimator–correlator with the MMSE signal estimator) and the MLR approaches will, in general, produce receivers with different performances. As mentioned above, only in very special cases will the ALR and MLR approaches result in equivalent LR tests. Thus, in most circumstances, *estimator–correlator receivers using the ML parameter estimates to arrive at the signal estimator, i.e., the MLR approach, will result in suboptimum performance relative to the ALR approach.*

A. ALR and MLR Structures

In generalizing the ALR and MLR two-hypothesis receivers to M hypothesis structures, we observe from Decision Rule (8) that the optimum test still involves comparison of a likelihood ratio, $\Lambda_i\left(r(t)\right) \stackrel{\Delta}{=} p\left(r(t)\,|H_i\right)/p\left(r(t)\,|H_0\right)$ (which now depends on which signal hypothesis is being considered), with a threshold. The specific structure of these receivers depends on the form of the $M-1$ signals representing the signal-plus-noise hypotheses. In line with the signal form assumed in [1], namely, a fixed amplitude sinusoid with either unknown phase and known frequency or both unknown phase and unknown frequency, we shall assume for the M-hypothesis case a set of $M-1$ sinusoids (at frequencies $f_{c,1}, f_{c,2}, \ldots, f_{c,M-1}$) with the same unknown parameters. Since the best performance with such a signaling set is achieved when the signals are equal energy and orthogonal, we shall make this further

[2] A short summary of the results in [2] as they apply to the two-hypothesis signal detection problem is presented in Appendix A. Examples are given for the cases of sinusoidal carrier with known frequency and unknown phase and for sinusoidal carrier with unknown phase and unknown frequency. Note that Kailath refers to what we call an average-likelihood ratio test as a generalized-likelihood ratio test.

assumption here.[3] Note, however, that the structures of the optimum ALR and MLR receivers do not require this orthogonality constraint. Without going into great detail, we summarize here the results for the specific cases treated in [1]. The reader is referred to [1] for more detail on the two-hypothesis case.

1. Sinusoidal Carriers With Unknown Phase and Known Frequency—ALR and MLR. The optimum ALR or MLR receiver computes for each of the $M-1$ transmitted frequencies the envelope

$$\left.\begin{aligned} L_i &= \sqrt{L_{ci}^2 + L_{si}^2} \\ L_{ci} &\triangleq \int_0^T r(t)\sqrt{2}\cos 2\pi f_{ci} t \; dt \\ L_{si} &\triangleq \int_0^T r(t)\sqrt{2}\sin 2\pi f_{ci} t \; dt, \quad i = 1, 2, \ldots, M-1 \end{aligned}\right\} \tag{12}$$

The decision rule in both cases is

> If $L_i^2 > \gamma$ for any i, choose hypothesis H_i (or equivalently $s_i(t)$) corresponding to $\max\limits_i L_i^2$.
>
> Otherwise ($L_i^2 \leq \gamma$ for all $i = 1, 2, \ldots, M-1$), choose hypothesis H_0 (corresponding to no signal sent).

In the MLR case, it is understood that the unknown carrier phase is to be replaced by its ML estimate for *each* of the conditional likelihood ratios, so that the decision rule is determined from a comparison of the set $\hat{\Lambda}_i(r(t)) = p(r(t)|\, H_i, \hat{\theta}_{iML})/p(r(t)|\, H_0)$, $i = 1, 2, \ldots, M-1$ with a threshold. Note that the ML phase estimate now depends on the hypothesis H_i. A receiver that implements the above decision rule is illustrated in Fig. 1.

2. Sinusoidal Carriers With Unknown Phase and Unknown Frequency—ALR. Assuming a frequency uncertainty region of $\pm B/2$ around each of the possible transmitted tones, then the optimum ALR receiver computes for each of the $M-1$ transmitted frequencies the quantity[4]

$$Y_i \triangleq \int_{f_{ci}-B/2}^{f_{ci}+B/2} I_0\left(\frac{2\sqrt{P}}{N_0} L(f)\right) df, \quad i = 1, 2, \ldots, M-1 \tag{13}$$

where $L(f)$ is defined analogously to Eq. (12) by

---

[3] The current proposal for a spacecraft-monitoring system assumes a signaling set composed of pairs of sinusoidal tones symmetrically placed around a carrier. These tones are generated by modulating a fixed carrier with a set of subcarriers. It is shown in Appendix B that, by proper selection of the subcarrier frequency spacing, such a signaling set can be made to satisfy the orthogonality constraint.

[4] We further assume that the nominal carrier frequencies of the tones are chosen sufficiently far apart so that the frequency uncertainty bands around each are nonoverlapping.

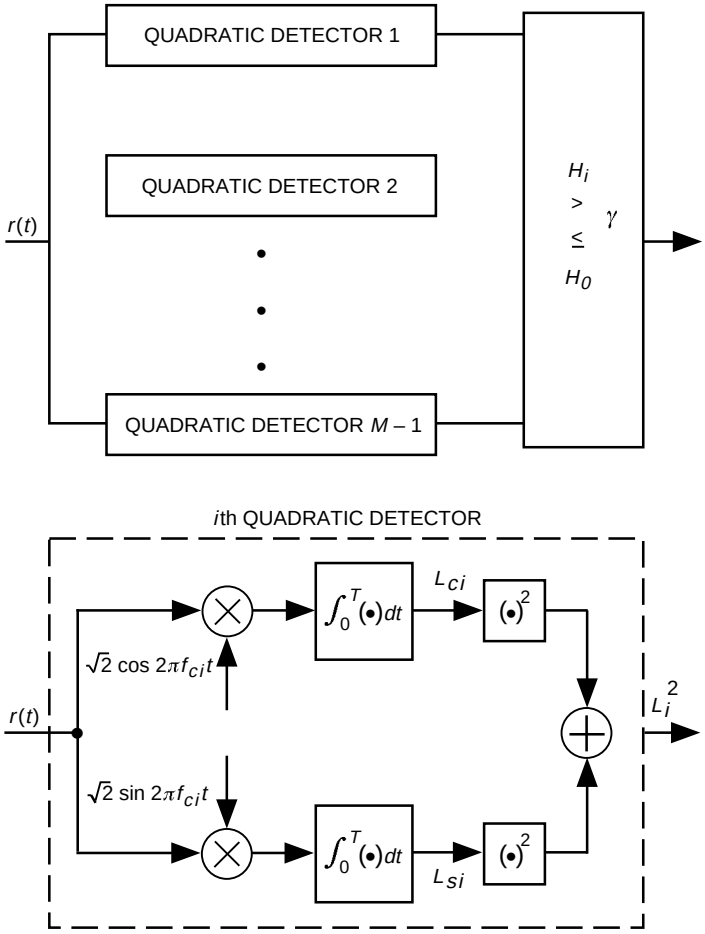

Fig. 1. ALR detector of $M-1$ sinusoidal tones with known frequency and unknown phase in additive white Gaussian noise (AWGN).

$$\left.\begin{aligned} L(f) &= \sqrt{L_c^2(f) + L_s^2(f)} \\ L_c(f) &\triangleq \int_0^T r(t)\sqrt{2}\cos 2\pi f t \; dt \\ L_s(f) &\triangleq \int_0^T r(t)\sqrt{2}\sin 2\pi f t \; dt \end{aligned}\right\} \tag{14}$$

The decision rule is

If $Y_i > \gamma$ for any i, choose hypothesis H_i (or equivalently $s_i(t)$) corresponding to $\max\limits_i Y_i$.

Otherwise ($Y_i \leq \gamma$ for all $i = 1, 2, \ldots, M-1$), choose hypothesis H_0 (corresponding to no signal sent).

Since Eq. (13) is overly demanding to implement, one discretizes each of the $M-1$ frequency uncertainty intervals into $G = B/T^{-1} = BT$ subintervals, to each of which is associated a candidate frequency $f_{ci,j},\ i = 1, 2, \ldots, M-1,\quad j = 0, 1, \ldots, G-1$ located at its center. Such a discretization results in orthogonal envelope detector outputs. As such, the integration over the continuous uncertainty regions in Eq. (13) is approximated by a discrete (Riemann) sum and, hence, the approximate statistic to be used in the decision rule is

$$Y_i \cong \sum_{j=0}^{G-1} I_0\left(\frac{2\sqrt{P}}{N_0} L(f_{ci,j})\right), \quad i = 1, 2, \ldots, M-1 \tag{15}$$

A receiver that implements the above decision rule is illustrated in Fig. 2.

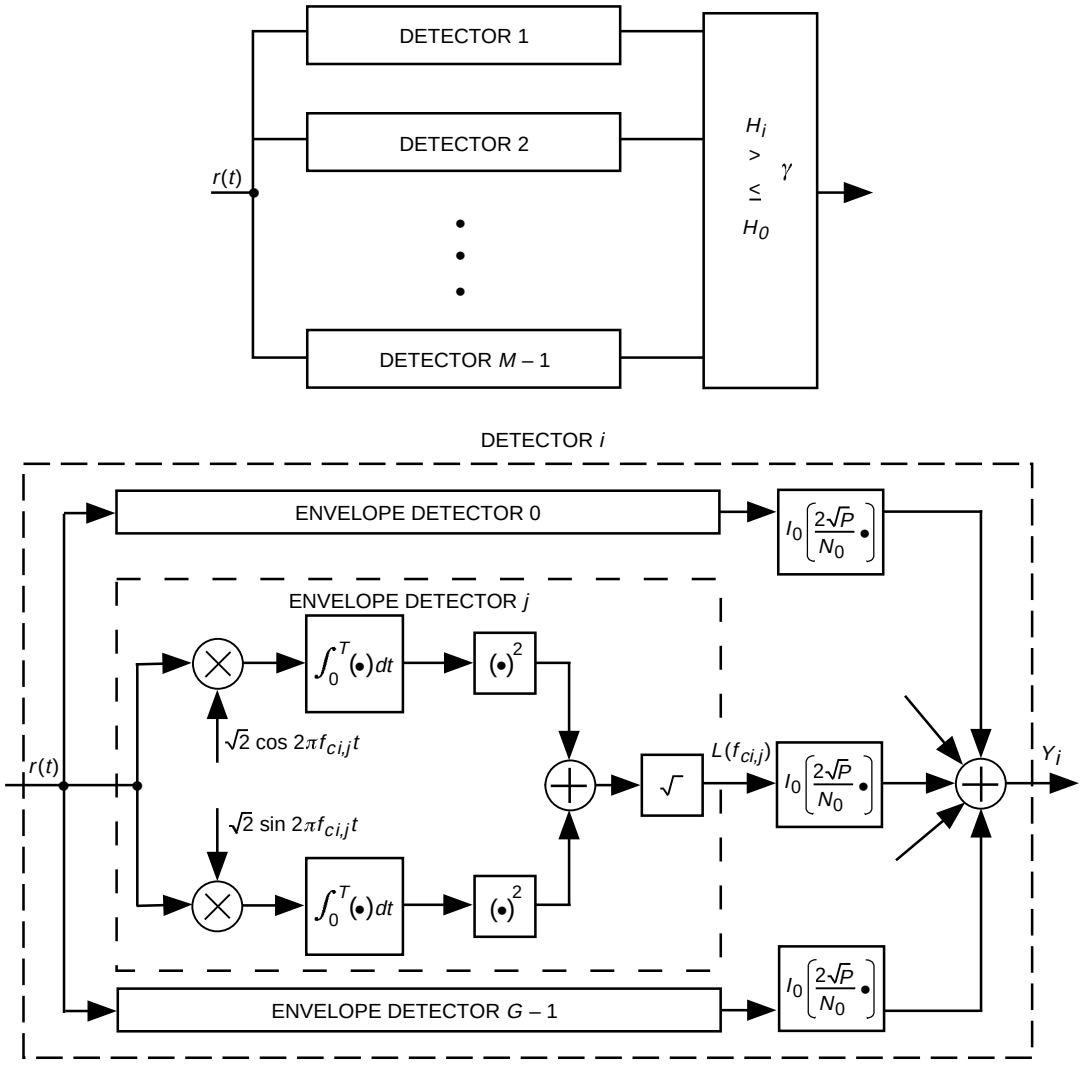

Fig. 2. ALR detection of $M-1$ sinusoidal tones with unknown frequency and unknown phase in AWGN.

3. Sinusoidal Carriers With Unknown Phase and Unknown Frequency—MLR. Again assuming disjoint frequency uncertainty regions of $\pm B/2$ around each of the possible transmitted tones, then the optimum MLR receiver computes for each of the $M-1$ transmitted frequencies the quantity

$$Y_i = \max_f L(f), \quad f_{ci} - \frac{B}{2} \le f \le f_{ci} + \frac{B}{2} \tag{16}$$

where $L(f)$ is defined in Eq. (14). The decision rule is the same as that following Eq. (14), namely,

> If $Y_i > \gamma$ for any i, choose hypothesis H_i (or equivalently $s_i(t)$) corresponding to $\max_i Y_i$.
>
> Otherwise ($Y_i \le \gamma$ for all $i = 1, 2, \ldots, M-1$), choose hypothesis H_0 (corresponding to no signal sent).

This rule results in a spectral maximum form of receiver. Again because of the excessive demand placed on the implementation by the need to evaluate Eq. (16) over a continuum of frequencies, we again quantize each of the frequency uncertainty regions into $G = BT$ subintervals, each with an associate candidate frequency $f_{ci,j}$, $i = 1, 2, \ldots, M-1$, $j = 0, 1, \ldots, G-1$ located at its center. As such, the frequency continuous test statistic of Eq. (16) can be approximated by the discrete form

$$Y_i = \max_j L\left(f_{ci,j}\right) \tag{17}$$

A receiver that implements the above decision rule is illustrated in Fig. 3.

Before going on to discuss the performance of these various structures as well as others that account for higher-order phase derivatives, e.g., frequency rate, we digress to reemphasize a point made in the introduction, namely, that from a *signal detection* (as opposed to *data communication*) point of view, the optimum (based on likelihood ratio considerations) receiver in the presence of unknown parameters is determined by averaging over the statistics of these parameters rather than by trying to estimate them with, for example, ML estimation. Structures that evolve from such considerations are noncoherent in nature. Even if one employs a structure that first estimates these parameters and then performs a pseudocoherent detection based on these parameter estimates, such as that suggested by the MLR approach, it is important to emphasize the fact that this approach requires that *the estimation and the detection operations take place over the same entire observation interval.* Any deviation from these considerations leads to a suboptimum receiver.

The reason for stressing the above points is that from time to time it has been suggested that a conventional coherent (actually pseudocoherent) BPSK receiver might be suitable for solving the spacecraft-monitoring problem. In particular, it has been suggested that the signals representing the hypotheses H_i, $i = 1, 2, \ldots, M-1$ be selected as a set of orthogonal bit streams at a rate of $1/T_b$ and that the unknown phase be tracked at the receiver by a carrier tracking loop, e.g., a Costas loop, to provide the necessary pseudocoherent demodulation reference signal. To put this proposal to rest once and for all, we discuss in the next section the detection performance of such a scheme and what system parameter requirements, e.g., carrier loop bandwidth, would be needed to make it operable in a region akin to that of the ALR and MLR structures.

B. Signal Detection Using Pseudocoherent BPSK and Orthogonal Bit Streams

Consider an orthogonal signaling set described by

$$s_i(t) = \sqrt{2P} m_i(t) \cos\left(\omega_c t + \theta\right), \quad i = 1, 2, \ldots, M-1 \tag{18}$$

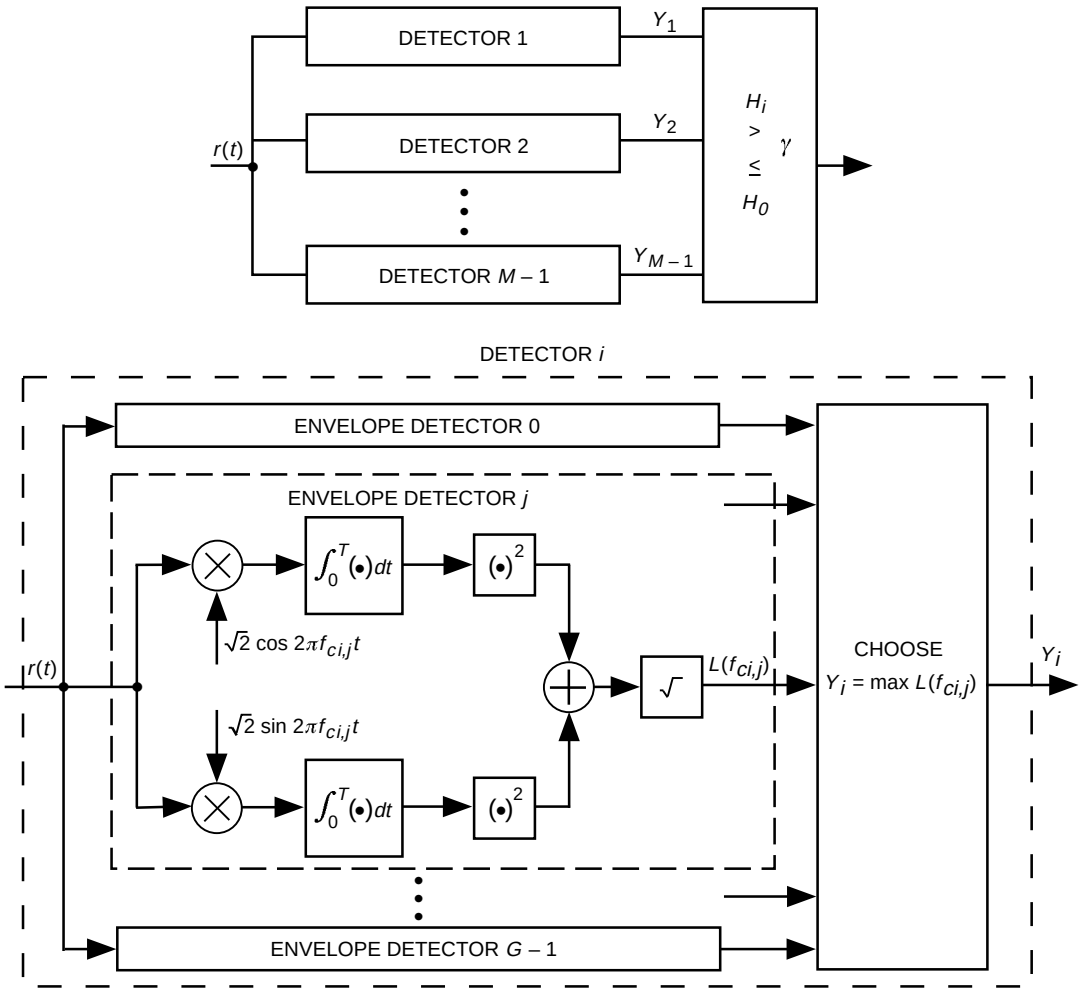

Fig. 3. MLR detection of $M-1$ sinusoidal tones with unknown frequency and unknown phase in AWGN.

where

$$m_i(t) = \sum_{k=1}^{K} c_{ik} p\,(t - nT_b), \quad i = 1, 2, \ldots, M-1 \tag{19}$$

with $p(t)$ a unit amplitude rectangular pulse of duration T_b, and the binary vectors $\mathbf{c}_i = [c_{i1}, c_{i2}, \ldots, c_{iK}]^T$ of length KT_b are orthogonal, i.e.,

$$\mathbf{c}_i^T \mathbf{c}_j = \begin{cases} 1, & i = j \\ 0, & i \neq j \end{cases} \tag{20}$$

The signals in Eq. (18) are assumed to represent the various noncatastrophic spacecraft states. Also, the observation time T for making a signal-present versus signal-absent determination is now equal to KT_b.

The receiver first derives a demodulation reference from a carrier tracking loop and then performs a matched-filter (correlation) detection of each of the possible transmitted waveforms. Analogous to

the type of decision rule previously derived for an M-hypothesis Neyman–Pearson test, if any of these matched outputs exceeds a threshold, then hypothesis H_i is chosen corresponding to the largest matched-filter output. If none of the matched-filter outputs exceeds the threshold, then the null hypothesis H_0 is chosen. An implementation of such a receiver is illustrated in Fig. 4.

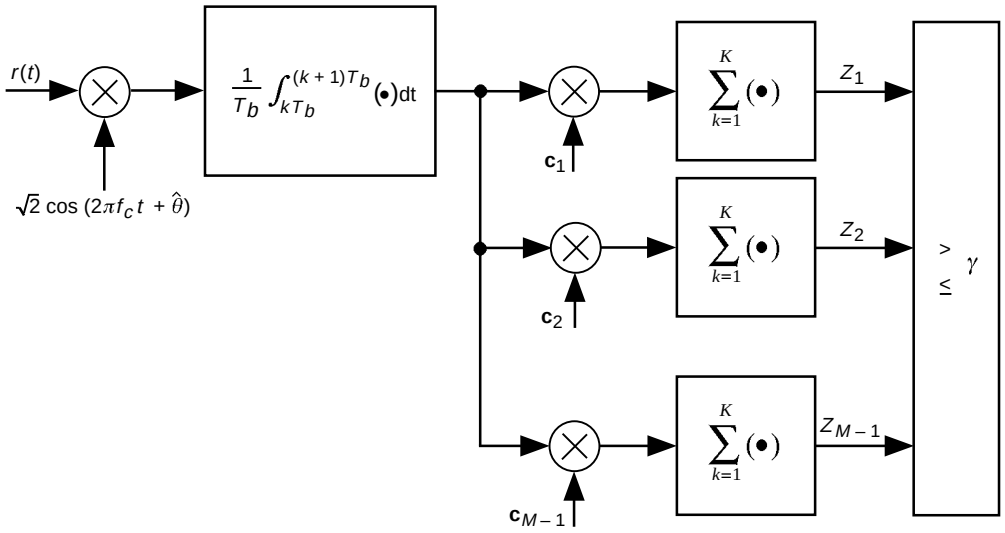

Fig. 4. Pseudocoherent receiver for signal detection with orthogonal BPSK waveforms.

The matched-filter outputs $Z_i,\ i = 1, 2, \ldots, M-1$ are Gaussian random variables described by

$$\left.\begin{aligned} Z_i|_{H_i} &= K\sqrt{P}\ \overline{\cos\phi_c} + \sum_{k=1}^{K} c_{ik}N_k \\ Z_j|_{H_i} &= \sum_{k=1}^{K} c_{jk}N_k, \quad j = 1, 2, \ldots, M-1, \quad j \neq i \end{aligned}\right\} \tag{21}$$

under hypothesis $H_i,\ i \neq 0$ and

$$Z_j\,|_{H_0} = \sum_{k=1}^{K} c_{jk}N_k, \quad j = 1, 2, \ldots, M-1 \tag{22}$$

under hypothesis H_0. In Eqs. (21) and (22), N_k are independent zero-mean Gaussian random variables with variance $\sigma^2 = N_0/2T_b$ representing the integrate-and-dump (I&D) output noise components in each of the K-bit intervals. Also, $\phi_c \triangleq \theta - \hat{\theta}$ denotes the carrier loop phase error, and the overbar denotes statistical average.

Under hypothesis H_0, the Z_j's are uncorrelated (because of the orthogonality of the data sequences) and, hence, independent (because they are Gaussian), i.e.,

$$E\left\{\left(Z_k - \overline{Z_k}\right)\left(Z_l - \overline{Z_l}\right)|H_0\right\} = \begin{cases} K\sigma^2 \triangleq \sigma_N^2, & k = l \\ 0, & k \neq l \end{cases} \tag{23}$$

Thus, the false alarm probability becomes

$$P_{FA} = 1 - \Pr\{Z_1, Z_2, \ldots, Z_{M-1} \leq \gamma \,|H_0\} = 1 - \left[\frac{1}{2}\ \text{erfc}\left(-\frac{\gamma}{\sqrt{2}\sigma_N}\right)\right]^{M-1}$$

$$= 1 - \left[1 - \frac{1}{2}\text{erfc}\left(\frac{\gamma}{\sqrt{2}\sigma_N}\right)\right]^{M-1} \tag{24}$$

where γ is the detection threshold.

Assuming now that $s_i(t)$ was transmitted (hypothesis H_i is in fact true), then using Eq. (21), the probability of detection, P_D, is evaluated as

$$P_D = \Pr\{Z_i > \gamma; Z_1, Z_2, \ldots, Z_{i-1}, Z_{i+1}, \ldots, Z_{M-1} \leq Z_i \,|H_i\}$$

$$= \int_\gamma^\infty \frac{1}{\sqrt{2\pi\sigma_N^2}} \exp\left\{-\frac{\left(Z_i - K\sqrt{P}\ \overline{\cos\phi}\right)}{2\sigma_N^2}\right\}\left[\frac{1}{2}\ \text{erfc}\left(-\frac{Z_i}{\sqrt{2}\sigma_N}\right)\right]^{M-2} dZ_i \tag{25}$$

Eliminating the threshold between Eqs. (24) and (25), the receiver operating characteristic (ROC) becomes, after simplification,

$$\left.\begin{aligned} P_D &= \frac{1}{\sqrt{\pi}}\int_\eta^\infty \exp\{-Y^2\}\left[1 - \frac{1}{2}\ \text{erfc}\left(Y + \sqrt{\frac{PT}{N_0}}\overline{\cos\phi}\right)\right]^{M-2} dY \\ \eta &= \text{erfc}^{-1}\left\{2\left[1 - (1 - P_{FA})^{1/(M-1)}\right]\right\} - \sqrt{\frac{PT}{N_0}}\overline{\cos\phi} \end{aligned}\right\} \tag{26}$$

For $M = 2$ (a two-hypothesis test), Eq. (26) reduces to

$$P_D = \frac{1}{2}\ \text{erfc}\ \eta = \frac{1}{2}\ \text{erfc}\left[\text{erfc}^{-1}\{2P_{FA}\} - \sqrt{\frac{PT}{N_0}}\overline{\cos\phi}\right] \tag{27}$$

Note that both Eqs. (26) and (27) do not explicitly depend on the bit time T_b or the number of bits K in the observation interval T, i.e., the length of the orthogonal sequences. Rather, what is important in the signal detection problem is the total energy PT in the observation.

To evaluate Eq. (26) or Eq. (27) numerically, we must relate the carrier tracking loop degradation factor $\overline{\cos\phi}$ to the parameters of the loop itself, such as loop SNR. For a carrier tracking loop with single-sided loop bandwidth B_L, the loop SNR is defined as $\rho = P/N_0B_L$. While this definition of loop bandwidth is exact for a phase-locked loop (PLL), for a suppressed-carrier loop such as a Costas loop, the definition should include the so-called "squaring loss," which is a factor less than unity and as such reduces the effective loop SNR. To keep matters simple, however, we shall ignore this difference and assume a PLL for carrier tracking. For such a loop, it is well-known [3] that the $\overline{\cos\phi}$ degradation factor is given by

$$\overline{\cos\phi} = \frac{I_1(\rho)}{I_0(\rho)} = \frac{I_1\left(\dfrac{PT}{N_0}\ \dfrac{1}{B_L T}\right)}{I_0\left(\dfrac{PT}{N_0}\ \dfrac{1}{B_L T}\right)} \tag{28}$$

where $I_n(x)$ is the nth-order modified Bessel function of the first kind. Substituting Eq. (28) into Eq. (26) or Eq. (27) allows one to compute the detection probability, P_D, as a function of detection SNR, $d^2 = 2PT/N_0$ (in dB) for fixed values of false alarm probability, P_{FA}, and observation time T, with loop bandwidth, B_L, as a parameter. Figure 5 presents such a plot for a two-hypothesis test with $P_{FA} = 10^{-2}$ and $T = 1000$ s. For comparison purposes, we present the comparable results for the optimum noncoherent ALR scheme, namely (see Eq. (18) of [1]),

$$P_D = Q\left(d, \sqrt{-2\ln P_{FA}}\right) \tag{29}$$

where $Q(\alpha, \beta)$ is Marcum's Q-function defined by

$$Q(\alpha, \beta) = \int_{\beta}^{\infty} z \exp\left(-\frac{z^2 + \alpha^2}{2}\right) I_0(\alpha z)\, dz \tag{30}$$

By inspection of the results in Fig. 5, we observe that, because of the large observation time, an impractically small loop bandwidth (e.g., $B_L = 0.002$ Hz) would be required to satisfy the PT/N_0 requirement necessary to achieve the performance comparable to the optimum noncoherent ALR detector. The intuitive reason for this can be gleaned from the optimum noncoherent MLR detector (whose performance is almost as good as that of the ALR), wherein the ML (open loop) estimate of the phase is obtained from the received signal over the entire observation interval. To obtain a phase estimate with a closed-loop

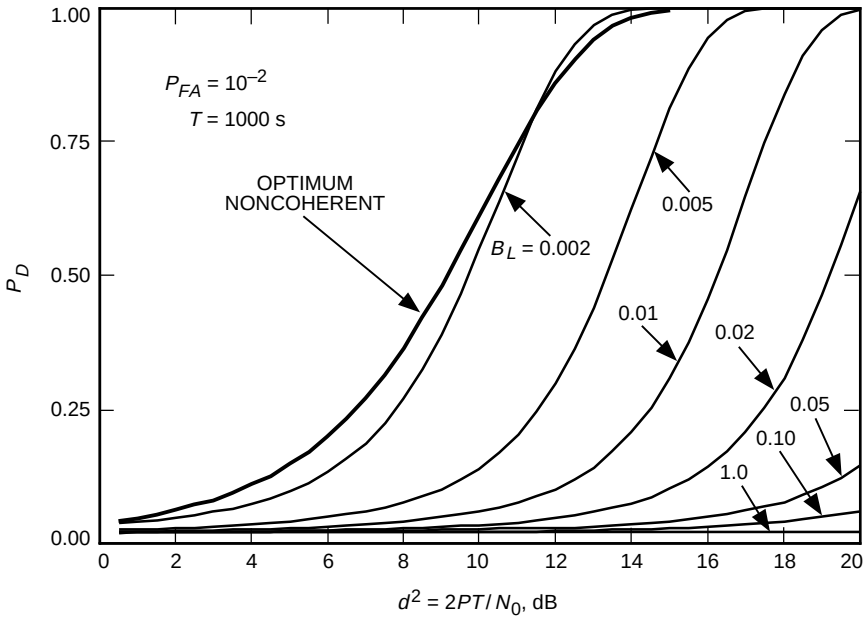

Fig. 5. Detection performance of the pseudocoherent PSK system using orthogonal sequences to represent the system states (hypotheses).

device with comparable accuracy, the loop bandwidth would have to be on the order of the reciprocal of the observation interval, which for $T = 1000$ s would require a loop bandwidth on the order of 0.001 Hz.

It is clear then that application of a pseudocoherent PSK system, which is commonly used and quite effective for communicating digital data, is not appropriate to the signal detection problem of interest here, where the detection threshold is set by the need to maintain a low false alarm probability. Although, for simplicity, the numerical example considered here was for a two-hypothesis case ($M = 2$), evaluation of Eq. (27) combined with Eq. (28) would similarly yield a performance requiring impractical loop parameters when compared with the appropriate multiple-hypothesis performance of the optimum ALR scheme.

C. Performance of the ALR and MLR Structures

The detection performance of the frequency discrete ALR receiver in Fig. 2 cannot be obtained in closed form due to its highly complex nonlinear structure. Despite its complexity, however, it is important to obtain the performance of this receiver since it serves as a benchmark against which the performance of any other simpler-to-implement structures (including those derived from MLR theory) can be compared. Thus, to obtain this performance, we shall resort to results obtained from computer simulations. In constructing the simulation for the signal-plus-noise hypotheses, a decision must be made regarding the selection of the true received frequency of the input signal. In making this selection, it is important to understand that spacing the frequencies $f_{ci,j}, j = 0, 1, 2, \ldots, G-1$ for each of the signal hypotheses $H_i,\ i = 1, 2, \ldots, M-1$ by $1/T$ guarantees independence of the noise components that appear at the output of each of the spectral estimate channels. However, orthogonality of the signal components of these same outputs depends on the true value of the received frequency relative to the discretized frequencies assumed for implementation of the receiver. That is, if the true received frequency happens to fall on one of the $f_{ci,j}$'s, then a signal component will appear only in the corresponding spectral estimate channel, i.e., all other channels will contain noise only. On the other hand, if the true received frequency falls somewhere between two of the $f_{ci,j}$'s, then we have loss of orthogonality in that a spillover of signal energy occurs in the neighboring spectral estimates. The worst-case spillover would occur when the true received frequency is midway between two of the $f_{ci,j}$'s. (If a fast Fourier transform (FFT) implementation is used, then the worst-case degradation can be ameliorated by zero padding to interpolate between the frequency samples.) In view of the above, we shall present both best-case and worst-case performance results corresponding, respectively, to selecting the true received frequency for the simulation identical to one of the $f_{ci,j}$'s and midway between two of the $f_{ci,j}$'s.

Figure 6 is a plot of miss probability $P_M = 1 - P_D$ versus P/N_0 in dB-Hz for an observation time $T = 1000$ s, a frequency uncertainty region $\pm B/2 = \pm 1000$ Hz (thus $G = BT = 2 \times 10^6$), a false alarm probability $P_{FA} = 2 \times 10^{-4}$, and $M = 5$ (four signal-plus-noise states representing specific spacecraft conditions and one noise-only state representing spacecraft failure). These values have been suggested as being typical of the spacecraft-monitoring application. Also shown in this figure are the corresponding results for the MLR receiver of Fig. 3, which can be obtained from a straightforward generalization of the analytical results in [1] to the case of $M > 2$. We observe from a comparison of the ALR and MLR results that the latter is inferior to the former by a P/N_0 amount on the order of 1 dB-Hz for either the best- or worst-case situation. In each case, the difference between best and worst performance is about 2 dB-Hz.

D. Low SNR Approximation of the ALR Structure

With reference to Eq. (15), we observe that to implement the optimum ALR structure derived from the assumptions of unknown carrier phase and unknown carrier frequency (uncertainty about the nominal carrier), one must build a receiver containing G envelope detectors and Bessel function nonlinearities. Although theoretically possible, the complexity of such a receiver for the spacecraft-monitoring application, where the frequency uncertainty interval, B, is on the order of 2 kHz and the observation

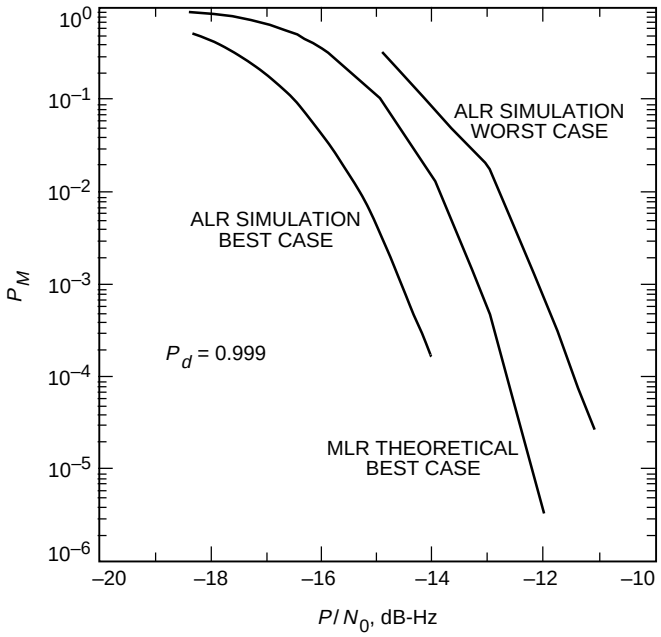

Fig. 6. The probability of miss, P_M, versus P/N_0 at P_f = 0.0002 for the MLR theory (best case) and ALR simulation (best and worst cases), where B = 2000 Hz, T = 1000 s ($G = 2 \times 10^6$), and M = 60,000.

time interval, T, is on the order of 1000 s, yielding $G = BT = 2 \times 10^6$, is simply too great. As such, we seek an alternate approach that combines this large bank of noncoherent processors into perhaps a single noncoherent processor, thus greatly reducing the implementation burden.

One such approach is obtained by approximating the $I_0(x)$ Bessel function by its small argument equivalent. In particular, for small values of x, we have $I_0(x) \cong 1 + 0.25x^2$. Of course, one could simply make this approximation for the Bessel functions in the discrete frequency form of the decision statistic as given by Eq. (15), which would suggest the low SNR ALR receiver of Fig. 7 (also see Figs. 7 through 11 of [4]). While this approach is useful in computing the approximate detection performance of the receiver (as we shall see shortly), unfortunately it only reduces the complexity per channel (by eliminating the need for the square root and Bessel function nonlinearities) but does not reduce the complexity in terms of the number of parallel channels needed. On the other hand, making the above Bessel function approximation in the continuous frequency form of the decision statistic as given by Eq. (13) together with Eq. (14) results in

$$Y_i \cong \int_{f_{ci}-B/2}^{f_{ci}+B/2} \left[1 + \frac{P}{N_0^2}\left(L_c^2(f) + L_s^2(f)\right)\right] df$$

$$= B + \frac{P}{N_0^2}\int_{f_{ci}-B/2}^{f_{ci}+B/2} \left(L_c^2(f) + L_s^2(f)\right) df, \quad i = 1, 2, \ldots, M-1 \tag{31}$$

Substituting for $L_c^2(f)$ and $L_s^2(f)$ from Eq. (14) gives

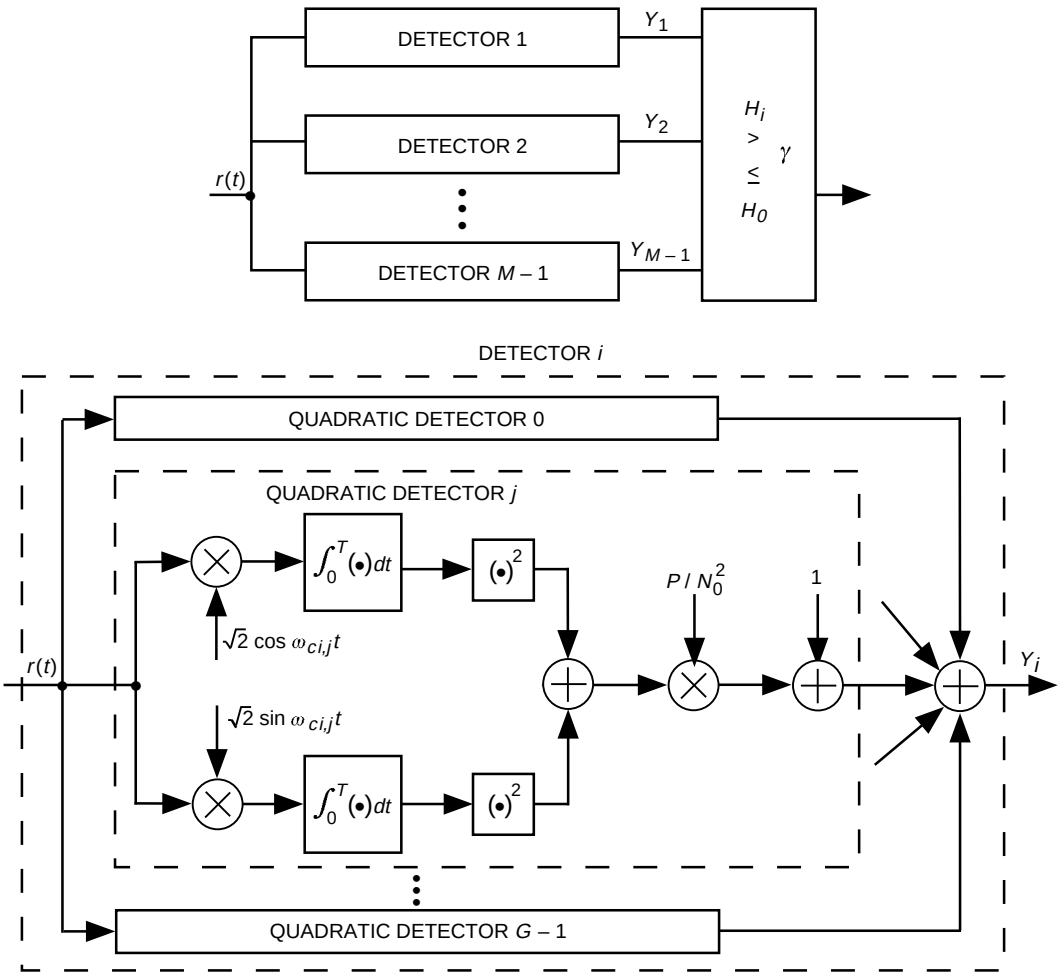

Fig. 7. Low SNR approximation to the ALR detection of $M-1$ sinusoidal tones with unknown frequency and unknown phase in AWGN.

$$Y_i \cong B + \frac{2P}{N_0^2}\int_{f_{ci}-B/2}^{f_{ci}+B/2}\int_0^T\int_0^T r(t)r(\tau)\cos 2\pi f t\cos 2\pi f\tau\, dt\, d\tau\, df$$

$$+\frac{2P}{N_0^2}\int_{f_{ci}-B/2}^{f_{ci}+B/2}\int_0^T\int_0^T r(t)r(\tau)\sin 2\pi f t\sin 2\pi f\tau\, dt\, d\tau\, df$$

$$= B + \frac{2P}{N_0^2}\int_0^T\int_0^T r(t)r(\tau)\left(\int_{f_{ci}-B/2}^{f_{ci}+B/2}\cos 2\pi f(t-\tau)df\right)dt\, d\tau \qquad (32)$$

Shifting the integration on f to the interval $(-B/2, B/2)$, and then performing this integration, Eq. (32) evaluates to

$$Y_i \cong B + \frac{P}{N_0^2}\int_0^T \int_0^T r(t)r(\tau)\cos 2\pi f_{ci}(t-\tau)\frac{B\sin\left[\pi B\left(t-\tau\right)\right]}{\pi B\left(t-\tau\right)}\,dt\,d\tau$$

$$= B + \frac{P}{N_0^2}\int_0^T r(t)\cos 2\pi f_{ci}t\left(\int_0^T r(\tau)\cos 2\pi f_{ci}\tau\frac{B\sin\left[\pi B\left(t-\tau\right)\right]}{\pi B\left(t-\tau\right)}d\tau\right)dt$$

$$+ \frac{P}{N_0^2}\int_0^T r(t)\sin 2\pi f_{ci}t\left(\int_0^T r(\tau)\sin 2\pi f_{ci}\tau\frac{B\sin\left[\pi B\left(t-\tau\right)\right]}{\pi B\left(t-\tau\right)}d\tau\right)dt \tag{33}$$

For $B >> 1/T$, i.e., a large BT product, as is the case of interest here, we can interpret the integrals on τ as the output of a unit amplitude rectangular lowpass filter of bandwidth B excited by the in-phase (I) and quadrature-phase (Q) demodulated (at frequency f_{ci}) input. Strictly speaking, this interpretation is only valid in the limit as $T \to \infty$. Denoting these filtered outputs by $y_c(t)$ and $y_s(t)$, we obtain a simple form for Eq. (33), namely,

$$Y_i \cong B + \frac{P}{N_0^2}\left[\int_0^T \left(r(t)\cos 2\pi f_{ci}t\right)y_c(t)dt + \int_0^T \left(r(t)\sin 2\pi f_{ci}t\right)y_s\left(t\right)dt\right] \tag{34}$$

which has the physical interpretation illustrated in Fig. 8(a). Note that this implementation has the advantage of replacing for each hypothesis an entire bank of G noncoherent processors with a *single* square-and-integrate processing. Since the wideband noise at the inputs to the rectangular filters in Fig. 8(a) can be separated into an in-band component (one whose energy lies in the interval $(-B/2, B/2)$) and a wide out-of-band component (one whose energy lies outside of $(-B/2, B/2)$), then for $B >> 1/T$, in so far as the T-sec I&D outputs are concerned, the product of the filter outputs and the wide out-of-band components can be ignored relative to the product of the filter outputs and the in-band components. As such, another approximate form of Eq. (33) is

$$Y_i \cong B + \frac{P}{N_0^2}\left[\int_0^T y_s^2(t)dt + \int_0^T y_c^2(t)dt\right] \tag{35}$$

which has the implementation of Fig. 8(b). It should be noted that, for any finite T, Eq. (34) will always yield better performance than Eq. (35); however, in the limit as $T \to \infty$, the two become equivalent. Since both Eqs. (34) and (35) are approximations to the true low SNR ALR statistic, Eq. (35) is the preferable one to use. Furthermore, as we shall soon see, in so far as detection performance is concerned, the rectangular filters of bandwidth B in Fig. 8(b) are only consequential in determining the number of independent samples (BT) contained in the observation time interval. That is, the performance will not explicitly depend on B or T individually, but rather on the product $G = BT$.

The performance of the low SNR approximation to the ALR illustrated in Fig. 7 (which also applies to the implementations in Fig. 8) can be approximately computed by applying a Gaussian assumption to the Y_i's. In particular, using the small argument approximation to the $I_0(x)$ function in Eq. (15), we have that

$$Y_i \cong \sum_{j=0}^{G-1}\left(1 + \frac{P}{N_0^2}L^2(f_{ci,j})\right) \triangleq G + Z_i, \quad i = 1, 2, \ldots, M-1 \tag{36}$$

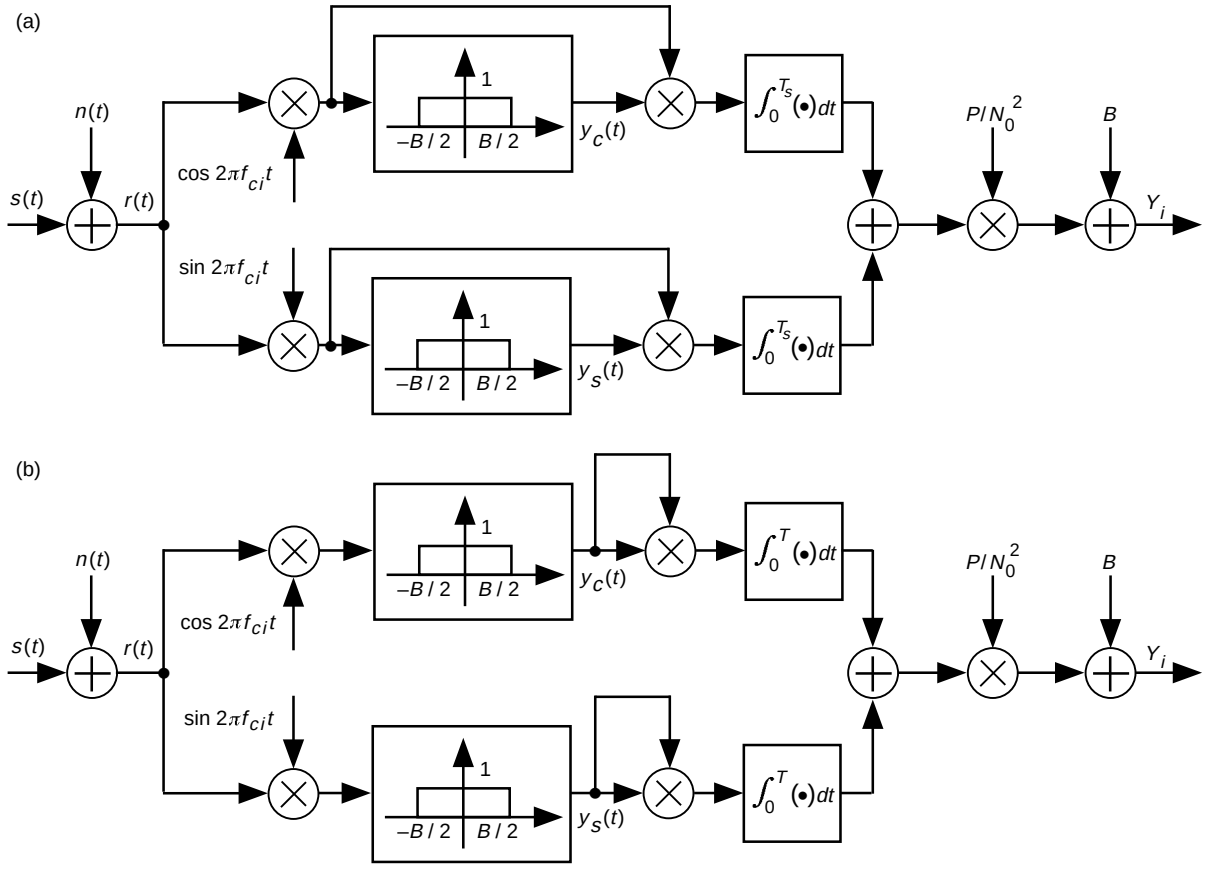

Fig. 8. Channel *i* noncoherent processors for a low SNR ALR receiver, from : (a) Eq. (34) and (b) Eq. (35).

Assuming that the transmitted signal is a sinusoid with random phase and frequency identically equal to one of the quantized frequencies of Eq. (36), then the mean and variance of Z_i under signal-plus-noise hypothesis (H_i) and noise only hypothesis (H_0) can be shown to be

$$E\{Z_i\} \triangleq \bar{Z} = \begin{cases} \dfrac{PT}{N_0}\left(\dfrac{PT}{N_0} + G\right), & H_i \\ \dfrac{PT}{N_0}G, & H_0 \end{cases}$$

$$\text{var}\ \{Z_i\} \triangleq \sigma_Z^2 = \begin{cases} \left(\dfrac{PT}{N_0}\right)^2\left(\dfrac{2PT}{N_0} + G\right), & H_i \\ \left(\dfrac{PT}{N_0}\right)^2 G, & H_0 \end{cases} \tag{37}$$

From the decision rule following Eq. (14), the false alarm probability is determined from the probability that all $M-1$ Y_i's are below the threshold γ under H_0. Equivalently, absorbing the constant G in Eq. (36) into the decision threshold and noting that the Y_i's are independent and, for large G, can be approximated as Gaussian, then analogously to Eq. (24), P_{FA} is determined from

$$P_{FA} = 1 - \Pr\{Y_1, Y_2, \ldots, Y_{M-1} \leq \gamma \,|H_0\} = 1 - \left[1 - \frac{1}{2}\text{erfc}\left(\frac{\gamma' - \bar{Z}\big|_{H_0}}{\sqrt{2}\,\sigma_Z|_{H_0}}\right)\right]^{M-1} \tag{38}$$

where $\gamma' \triangleq \gamma - G$ and $\bar{Z}\big|_{H_0}, \sigma_Z|_{H_0}$ are determined from Eq. (37). Similarly, since under the signal-plus-noise hypothesis only one of the Y_i's contains the signal, then analogously to Eq. (25), the detection probability is given by

$$\begin{aligned} P_D = &\Pr\{Y_i > \gamma; Y_1, Y_2, \ldots, Y_{i-1}, Y_{i+1}, \ldots, Y_{M-1} \leq Y_i |\, H_i\} \\ = &\int_{\gamma'}^{\infty} \frac{1}{\sqrt{2\pi\,\sigma_Z^2|_{H_i}}} \exp\left\{-\frac{\left(Z_i - \bar{Z}\big|_{H_i}\right)^2}{2\,\sigma_Z^2|_{H_i}}\right\}\left[1 - \frac{1}{2}\,\text{erfc}\left(\frac{Z_i - \bar{Z}\big|_{H_0}}{\sqrt{2}\,\sigma_Z|_{H_0}}\right)\right]^{M-2} dZ_i \end{aligned} \tag{39}$$

where, in addition to the above, $\bar{Z}\big|_{H_i}, \sigma_Z|_{H_i}$ are determined from Eq. (37). Eliminating the normalized threshold between Eqs. (38) and (39) and making use of the moments in Eq. (37), the ROC for the low SNR ALR receiver is approximately (based on a Gaussian model for the Y_i's) given by

$$\begin{aligned} P_D &= \frac{1}{\sqrt{\pi}}\frac{\sigma_Z|_{H_0}}{\sigma_Z|_{H_i}} \int_{\eta}^{\infty} \exp\left\{-\frac{\left(Y\sqrt{2}\,\sigma_Z|_{H_0} + \bar{Z}\big|_{H_0} - \bar{Z}\big|_{H_i}\right)^2}{2\,\sigma_Z^2|_{H_i}}\right\}\left[1 - \frac{1}{2}\,\text{erfc}\,Y\right]^{M-2} dY \\ &= \frac{1}{\sqrt{\pi}}\sqrt{\frac{G}{2PT/N_0 + G}} \int_{\eta}^{\infty} \exp\left\{-\left(\frac{G}{2PT/N_0 + G}\right)\left(Y - \frac{PT/N_0}{\sqrt{2G}}\right)^2\right\}\left[1 - \frac{1}{2}\,\text{erfc}\,Y\right]^{M-2} dY \\ \eta &\triangleq \text{erfc}^{-1}\left\{2\left[1 - (1 - P_{FA})^{\frac{1}{M-1}}\right]\right\} \end{aligned} \tag{40a}$$

For $G >> PT/N_0$ and $P_{FA} << 1$ (the cases of interest here), Eq. (40a) simplifies to

$$\left.\begin{aligned} P_D &= \frac{1}{\sqrt{\pi}} \int_{\eta}^{\infty} \exp\left\{-\left(Y - \frac{PT/N_0}{\sqrt{2G}}\right)^2\right\}\left[1 - \frac{1}{2}\,\text{erfc}\,Y\right]^{M-2} dY \\ \eta &\triangleq \text{erfc}^{-1}\left\{\left(\frac{1}{M-1}\right) 2P_{FA}\right\} \end{aligned}\right\} \tag{40b}$$

Furthermore, for the two-hypothesis problem, i.e., $M = 2$, Eq. (40a) simplifies to

$$P_D = \frac{1}{2}\,\text{erfc}\,\left[\sqrt{\frac{G}{2PT/N_0 + G}}\left(\text{erfc}^{-1}(2P_{FA}) - \frac{PT/N_0}{\sqrt{2G}}\right)\right] \cong \frac{1}{2}\,\text{erfc}\left[\text{erfc}^{-1}(2P_{FA}) - \frac{PT/N_0}{\sqrt{2G}}\right] \tag{41}$$

Figure 9 is a plot of miss probability $P_M = 1 - P_D$ as determined from Eqs. (40) and (41) versus P/N_0 in dB-Hz for the same parameters as in Fig. 6. The performance curves for the full-band receiver were obtained numerically from Eq. (40a) and the exact form of Eq. (41). For $M = 2$, these results were verified using the simulation technique described in Appendix C and are also illustrated in Fig. 9. Comparing Fig. 9 with the ALR results in Fig. 7, we observe the huge penalty in performance paid for the simplicity of implementation afforded by the low SNR approximation.

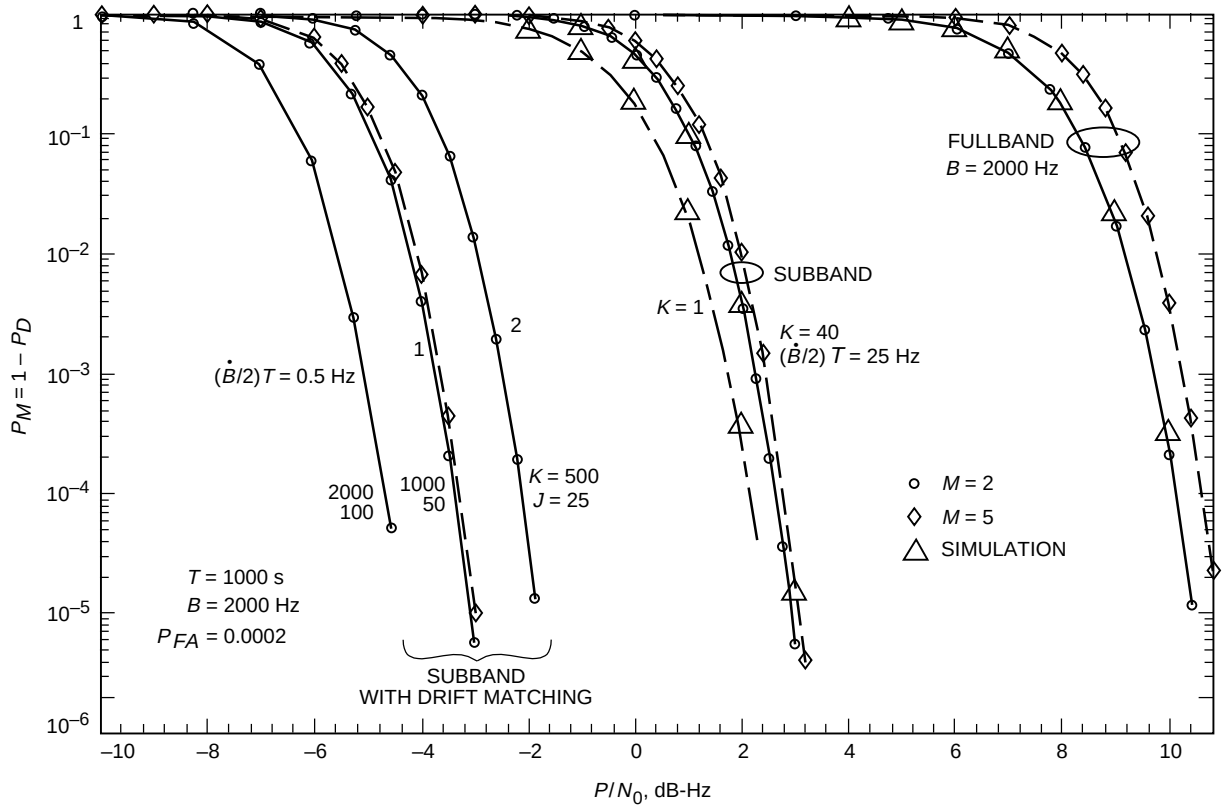

Fig. 9. The performance of squaring receiver structures.

E. ALR and MLR Structures for Sinusoidal Carriers With Unknown Phase, Frequency, and Frequency Rate

Assume now that, in addition to the uncertainty in phase and frequency of the transmitted sinusoidal carrier considered in Section III.A, there also exists an uncertainty in frequency rate corresponding to the presence of oscillator drift. If this drift is modeled as a linear variation in frequency over the observation interval, i.e., a constant but unknown frequency rate uniformly distributed in the interval $\pm\dot{B}/2$, then, following the ALR approach, it is straightforward to show that, analogously to Eq. (13), the optimum receiver computes for each of the $M-1$ transmitted frequencies the quantity

$$Y_i \triangleq \int_{-\dot{B}/2}^{\dot{B}/2} \int_{f_{ci}-B/2}^{f_{ci}+B/2} I_0\left(\frac{2\sqrt{P}}{N_0} L(f,\dot{f})\right) df\, d\dot{f}, \quad i = 1, 2, \ldots, M-1 \tag{42}$$

where

$$\left.\begin{aligned} L(f,\dot{f}) &= \sqrt{L_c^2(f,\dot{f}) + L_s^2(f,\dot{f})} \\ L_c(f,\dot{f}) &\triangleq \int_0^T r(t)\sqrt{2}\cos\left[2\pi\left(ft + \frac{1}{2}\dot{f}t^2\right)\right]dt \\ L_s(f,\dot{f}) &\triangleq \int_0^T r(t)\sqrt{2}\sin\left[2\pi\left(ft + \frac{1}{2}\dot{f}t^2\right)\right]dt \end{aligned}\right\} \tag{43}$$

The decision rule is still the same as that following Eq. (14). Since Eq. (42) is even more overly demanding to implement than was Eq. (13) because of the additional integration on $\dot{f}$, then once again we must resort to discretization of the frequency and frequency rate uncertainty intervals, resulting in the approximate decision variables

$$Y_i \triangleq \sum_{j=0}^{G-1}\sum_{l=0}^{F-1} I_0\left(\frac{2\sqrt{P}}{N_0}L(f_{ci,j},\dot{f}_l)\right), \quad i = 1,2,\ldots,M-1 \tag{44}$$

where $F \triangleq \dot{B}T^2/2$.[5] An illustration of an ALR receiver that employs this decision statistic is illustrated in Fig. 10.

In the presence of linear frequency drift, the optimum MLR receiver would compute for each of the $M-1$ transmitted frequencies the quantity

$$Y_i = \max_{f,\dot{f}} L(f,\dot{f}), \quad f_{ci} - \frac{B}{2} \le f \le f_{ci} + \frac{B}{2}, \quad -\frac{\dot{B}}{2} \le \dot{f} \le \frac{\dot{B}}{2} \tag{45}$$

and then apply the decision rule following Eq. (16). In discretized form, Eq. (45) would become [analogous to Eq. (17)]

$$Y_i = \max_{j,l} L(f_{ci,j},\dot{f}_l) \tag{46}$$

F. Low SNR Approximation of the ALR Structure

As in Section III.D, one can approximate the zero-order modified Bessel function in Eq. (44) by the first two terms in its power series. When this is done, then using Eq. (43), it is straightforward to show that, analogously to Eq. (33), one obtains

[5] The value of F, i.e., the quantization of the $\dot{f}$ uncertainty, is determined from approximate orthogonality considerations (see Appendix D).

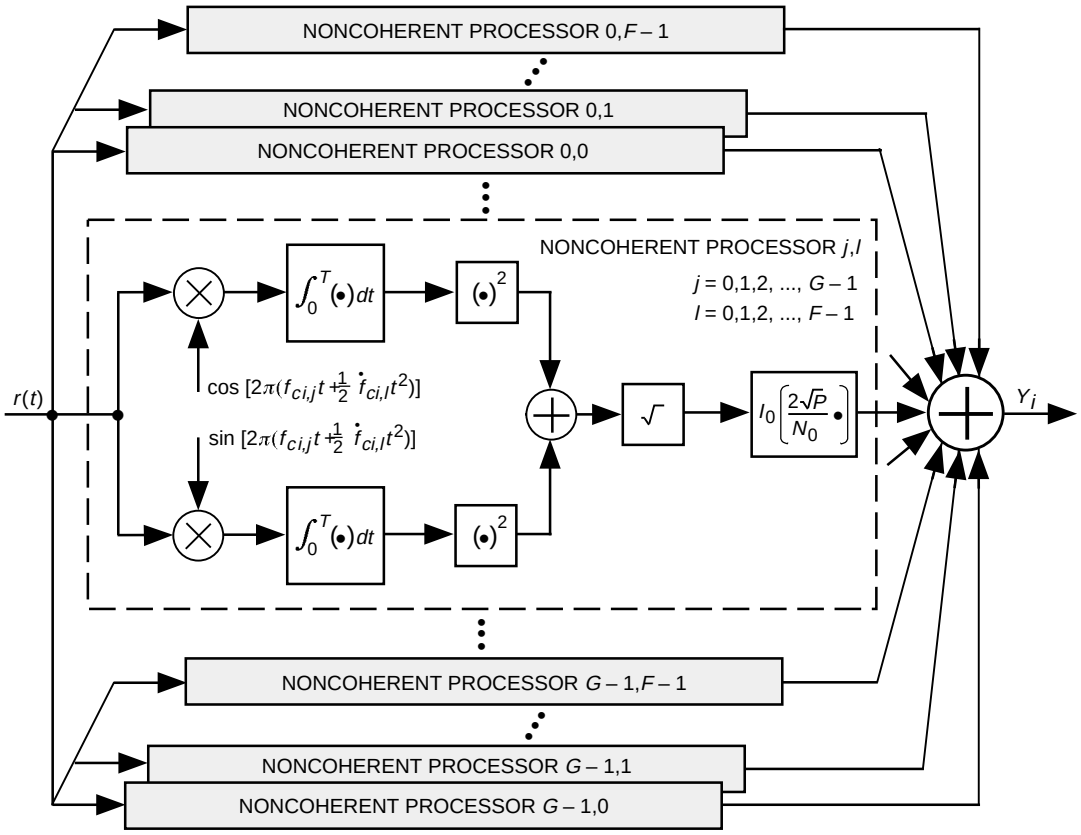

Fig. 10. The channel *i* ALR detector for detection of *M* – 1 sinusoidal tones with unknown phase, frequency, and frequency rate in AWGN.

$$Y_i \cong B\dot{B} + \frac{P}{N_0^2}\int_0^T r(t)\cos 2\pi f_{ci}t\left(\int_0^T r(\tau)\cos 2\pi f_{ci}\tau\frac{B\sin\left[\pi B\left(t-\tau\right)\right]}{\pi B\left(t-\tau\right)}\frac{\dot{B}\sin\left[\frac{\pi\dot{B}}{2}\left(t^2-\tau^2\right)\right]}{\frac{\pi\dot{B}}{2}\left(t^2-\tau^2\right)}d\tau\right)dt$$

$$+\frac{P}{N_0^2}\int_0^T r(t)\sin 2\pi f_{ci}t\left(\int_0^T r(\tau)\sin 2\pi f_{ci}\tau\frac{B\sin\left[\pi B\left(t-\tau\right)\right]}{\pi B\left(t-\tau\right)}\frac{\dot{B}\sin\left[\frac{\pi\dot{B}}{2}\left(t^2-\tau^2\right)\right]}{\frac{\pi\dot{B}}{2}\left(t^2-\tau^2\right)}d\tau\right)dt \qquad (47)$$

Unfortunately, Eq. (47) does not lend itself to an easy interpretation in terms of an implementation. However, if $(\dot{B}/2)T < B/2$ (i.e., the maximum frequency change due to drift is within the initial baseband frequency uncertainty interval), then over the observation interval, the $\sin y/y$ term involving $\dot{B}$ in Eq. (47) is much slower varying than the $\sin x/x$ term involving B and, to a first-order approximation, the former can be treated as a constant with respect to the time duration of the latter. As such, the implementations of Figs. 8(a) and 8(b) are still appropriate for the low SNR approximation to the ALR in the presence of linear frequency drift. Also invoking the Gaussian approximation to the statistics of Eq. (47), then to a first-order approximation, the detection performance is still given by Eqs. (40) and (41).

G. Improved Simple Receiver Structures for Signals With Bounded Frequency Drift

While the square-and-integrate receivers of Fig. 8 have the advantage that their simple structure and performance are approximately invariant to the presence of frequency drift, as previously mentioned, they pay a large penalty in performance when compared with the true optimum ALR schemes.[6] In an effort to improve upon this situation, we shall suggest a modification of the simple square-and-integrate receiver of Fig. 8(b) by exploiting the fact that, in the case of interest here, $\left(\dot{B}/2\right)T << B/2$, i.e., the drift over the observation interval is only a small fraction of the total initial frequency uncertainty band. In particular, typical spacecraft oscillators have a maximum one-sided drift rate on the order of 25 Hz in 1000 s, and thus for an observation time of $T = 1000$ s, $\left(\dot{B}/2\right)T = 25$ Hz, which is quite small compared with the assumed baseband frequency uncertainty interval of $B/2 = 1000$ Hz.

Consider dividing the total baseband frequency-uncertainty band $B/2$ Hz into K subbands of width $(\dot{B}/2)T$ Hz each, i.e., $K = (B/2)/(\dot{B}/2)T$, which for our ongoing example yields $K = 1000/25 = 40$. A motivation for doing this can be obtained by examining the behavior of the ALR structure of Fig. 2 when the input frequency drifts and is discussed following the end of this paragraph. The received signal in each of these subbands is squared-and-integrated in the manner of Fig. 8(b).[7] The maximum of these squared-and-integrated values (energies) is selected and compared to a threshold set by the requirement on false alarm probability. A receiver implementation based on M channels of the type described above (see Fig. 11) will be referred to herein as a subband squaring receiver, as contrasted with a full-band squaring receiver, which would incorporate M channels of the type illustrated in Fig. 8(b).

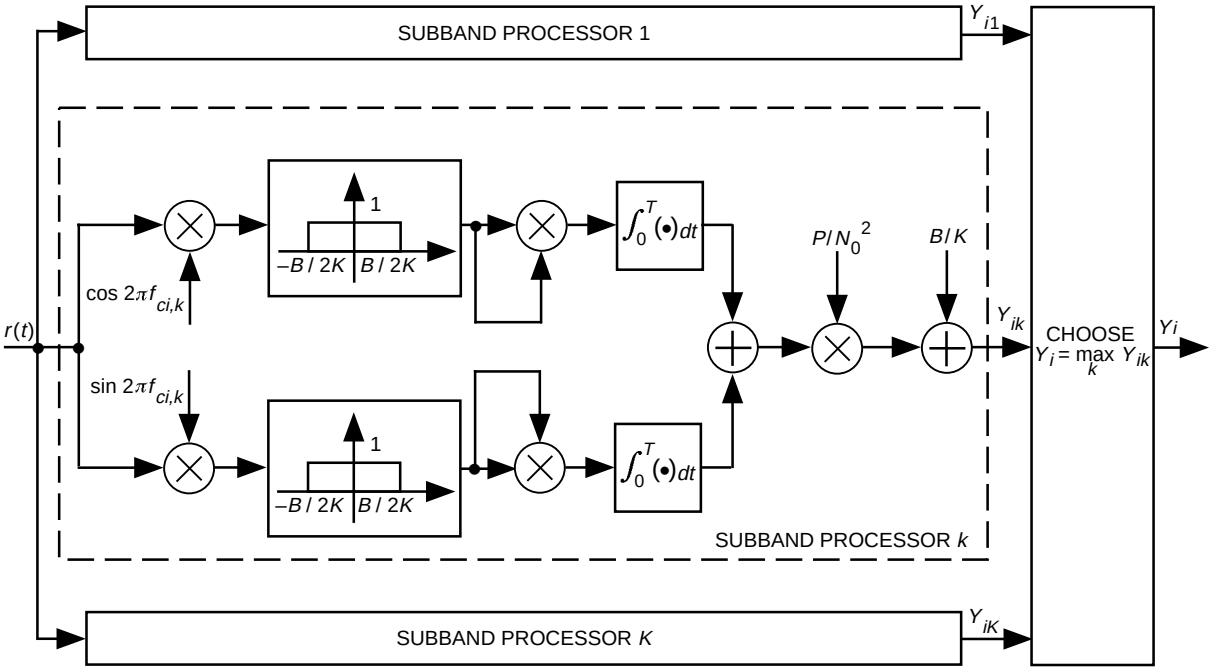

Fig. 11. The channel *i* noncoherent processor for the subband receiver.

[6] While is is true that the performances of the optimum ALR and MLR structures derived in Sections III.A.2 and III.A.3 and illustrated in Figs. 2 and 3 will degrade in the presence of drift approaching that of the simple receivers of Fig. 8, this will be less true for the optimum ALR and MLR structures derived in the presence of drift as described by the decision statistics in Section III.F.

[7] From an implementation point of view, the received signal is passed through a bank of disjoint subband bandpass filters, each of which can be implemented alternately as an I–Q demodulation with the carrier frequency at the center of the subband, followed by a baseband rectangular filter of width $(\dot{B}/2)T = B/2K$.

The construction of the subband squaring receiver can be motivated by reexamining the basic building block of the ALR receiver in Fig. 2, namely, the envelope detector. In particular, rewriting the squared envelope of the ijth detector as

$$L^2\left(f_{ci,j}\right) = \left[\int_0^T r(t)\sqrt{2}\cos 2\pi f_{ci,j}t\, dt\right]^2 + \left[\int_0^T r(t)\sqrt{2}\sin 2\pi f_{ci,j}t\, dt\right]^2$$

$$= \left|\int_0^T r(t)\sqrt{2}e^{-j2\pi f_{ci,j}t}\, dt\right|^2 = \left|\int_{-\infty}^{\infty} r(t)p(t)\sqrt{2}e^{-j2\pi f_{ci,j}t}\, dt\right|^2$$

where $p(t)$ is a unit amplitude rectangular pulse in the interval $0 \le t \le T$, shows that $L^2(f_{ci,j})$ can be interpreted as the energy component of the windowed signal $r(t)p(t)$ at frequency $f_{ci,j}$ over an effective bandwidth of $1/T$ Hz (the result of frequency domain spreading due to the finite duration of the time window $p(t)$). Thus, each envelope detector in Fig. 2 measures the energy in a narrow frequency band within the uncertainty band of interest. Since the center frequencies of adjacent envelope detectors are separated by $1/T$ Hz, it is clear that the ith detector in Fig. 2 consists of a bank of narrowband filters that completely covers the frequency uncertainty region associated with the ith signal. For a square window function, the frequency response of each filter is of the form $\sin x/x$, implying orthogonal outputs when the center frequencies are separated by $1/T$ Hz. Thus, the filter bank generates the maximum number of independent samples, BT, consistent with a bandwidth of B Hz and integration time of T s.

The MLR algorithm selects the largest energy component within the ith filter bank as the test statistic Y_i, as illustrated in Fig. 3. For the ALR algorithm, however, the energy components collected at each frequency are further processed by taking the square root, applying a scale factor, and computing the Bessel function $I_0(x)$ of the resulting scaled envelope. Following this, the results are summed to obtain the test statistic Y_i. Although the MLR structure is suboptimum, its performance is only slightly worse than that of the ALR algorithm for this application. Both the ALR and MLR structures are predicated on the assumption that the signal remains constant in frequency, which further implies that it remains within the passband of the same filter (channel) through the entire observation interval, ensuring the greatest possible SNR at the output of that filter. Equivalently, in terms of a changing input frequency, a maximum signal drift of less than $1/T$ Hz over the T-second observation is implied.

If the maximum frequency drift exceeds $1/T$ Hz during the observation, then the signal moves from one filter to the next, possibly spanning a large number of filters (channels) over the observation interval. In that case, no single filter contains all of the signal energy, which is now distributed among many adjacent filters. However, if the starting frequency and maximum drift rate were known, then the signal energy could still be recovered by combining (summing) the outputs of all filters spanned by the signal. Since the actual starting frequency is not known, this suggests using a filter bank with filter bandwidths large enough to accommodate the drifting signal. Thus, analogously to the ALR approach, we partition the uncertainty region into $K = BT/N$ (where N is an integer chosen in accordance with the maximum drift rate) filters, each of bandwidth N/T Hz, instead of BT filters of bandwidth $1/T$ Hz, as was done for the discrete version of the ALR with no frequency drift. The outputs of each subband filter are squared and integrated as shown in Fig. 11. Next, if we were to parallel the development of the ALR structure, we would take the square root of the outputs of each of these larger bandwidth (subband) filters, scale them, compute the Bessel function $I_0(x)$ of the resulting scaled envelopes, and sum to obtain the test statistic. We shall consider instead selecting the largest subband filter output within the ith detector as the test statistic for the corresponding ith hypothesis, analogous to what is done in the MLR structure.

For the system parameters of interest, the subband squaring receiver achieves a dramatic performance improvement over the full-band squaring receiver, primarily due to the reduced noise power in the subbands (each has only $1/K$ of the total noise power) degraded somewhat by occasional errors in selecting

the correct subband. Assuming a value of $K = 40$, an illustration of this performance improvement is superimposed on the full-band squaring receiver results in Fig. 9. The curve labeled $K = 1$ near the subband performance curves represents the performance of a full-band receiver with uncertainty bandwidth $B = 50$ Hz, and is used to illustrate the small amount of degradation due to choosing among 40 subbands. Note that the additional degradation caused by choosing between five hypotheses instead of two is negligibly small for this case. The subband performance curves were computed using Eqs. (52) and (55) (to be derived shortly), and the two-hypothesis case ($M = 2$) was verified using the simulation described in Appendix C. Comparing these results with those obtained for the full-band receiver, we observe a dramatic improvement in performance that is on the order of 7 dB. The analysis used to obtain these results assumes that the tones start at the boundary between subbands and drift (at no greater rate than their maximum rate) to the boundary of the adjacent subband in either the positive or negative direction from their starting points. As such, the received tone remains within a given subband over the entire observation interval. The details of the analysis are as follows.

The detection performance of the subband squaring receiver is obtained using a Gaussian approximation analogous to that employed for the full-band squaring receiver. In particular, since each of the K subband processors in Fig. 11 is implemented as in Fig. 8(b) but with lowpass rectangular filters that are $1/K$th the bandwidth, then the processor outputs $Y_{ik} \triangleq G/K + Z_{1k},\ k = 1, 2, \ldots, K$ can be modeled as independent Gaussian random variables with means and variances of Z_{1k}, as in Eq. (37) but with G replaced by G/K. Assuming first the two-hypothesis case, the probability of false alarm, P_{FA}, is equal to the probability that any of the K subband processor outputs exceeds the threshold under H_0. Equivalently, P_{FA} is equal to one minus the probability that none of the subband processor outputs exceeds the threshold under H_0, which is the same as one minus the probability that the maximum of the subband processor outputs does not exceed the threshold under H_0. Thus, analogously to Eq. (38),

$$P_{FA} = 1 - \Pr\{Y_1 \le \gamma \,|H_0\} = 1 - \left[1 - \frac{1}{2}\,\mathrm{erfc}\left(\frac{\gamma'' - \bar{Z}\big|_{H_0}}{\sqrt{2}\,\sigma_Z|_{H_0}}\right)\right]^K \tag{48}$$

where $\gamma'' = \gamma - G/K$, and from the above discussion,

$$\left.\begin{aligned} \bar{Z}\big|_{H_0} &= \left(\frac{PT}{N_0}\right)\left(\frac{G}{K}\right) \\ \sigma_Z|_{H_0} &= \left(\frac{PT}{N_0}\right)\sqrt{\frac{G}{K}} \end{aligned}\right\} \tag{49}$$

The missed detection probability, P_M, is the probability that the maximum of the subband processor outputs does not exceed the threshold under H_1, which, from the above, is equivalent to the the probability that none of the subband processor outputs exceeds the threshold under H_1. Thus, the correct detection probability, $P_D = 1 - P_M$, is given by

$$\begin{aligned} P_D &= 1 - \Pr\{Y_1 \le \gamma \,|H_1\} \\ &= 1 - \left[1 - \frac{1}{2}\,\mathrm{erfc}\left(\frac{\gamma'' - \bar{Z}\big|_{H_1}}{\sqrt{2}\,\sigma_Z|_{H_1}}\right)\right]\left[1 - \frac{1}{2}\,\mathrm{erfc}\left(\frac{\gamma'' - \bar{Z}\big|_{H_0}}{\sqrt{2}\,\sigma_Z|_{H_0}}\right)\right]^{K-1} \end{aligned} \tag{50}$$

where now

$$\left.\begin{aligned} \bar{Z}\big|_{H_1} &= \left(\frac{PT}{N_0}\right)\left(\frac{PT}{N_0}+\frac{G}{K}\right) \\ \sigma_Z\big|_{H_1} &= \left(\frac{PT}{N_0}\right)\sqrt{\frac{2PT}{N_0}+\frac{G}{K}} \end{aligned}\right\} \tag{51}$$

Note that Eq. (50) differs in form from Eq. (39) since here a correct detection occurs if *any* of the subband processor outputs exceeds the threshold, not necessarily only the one that contains the signal. In detecting among many hypotheses, as in Eq. (39), a correct detection only occurs if the particular full-band processor output that contains the signal exceeds the threshold. Eliminating the threshold between Eqs. (48) and (50) and making use of the moments in Eqs. (49) and (51) gives the two-hypothesis ROC as

$$P_D = 1-[1-P_{FA}]^{(K-1)/K} \times\left[1-\frac{1}{2}\ \mathrm{erfc}\left\{\sqrt{\frac{G/K}{2PT/N_0+G/K}}\left(\mathrm{erfc}^{-1}\left(2\left[1-(1-P_{FA})^{1/K}\right]\right)-\frac{PT/N_0}{\sqrt{2G/K}}\right)\right\}\right] \tag{52}$$

For $K=1$, i.e., the full-band squaring receiver, Eq. (52) reduces to Eq. (41) as it should.

For the M-hypothesis case, the probability of false alarm, P_{FA}, is given by

$$P_{FA} = 1-\Pr\{Y_1,Y_2,\ldots,Y_{M-1}\le\gamma\,|H_0\} = 1-\left[1-\frac{1}{2}\ \mathrm{erfc}\left(\frac{\gamma''-\bar{Z}\big|_{H_0}}{\sqrt{2}\,\sigma_Z|_{H_0}}\right)\right]^{K(M-1)} \tag{53}$$

where $\bar{Z}\big|_{H_0}$ and $\sigma_Z|_{H_0}$ are as defined in Eq. (49). Similarly to Eq. (39), the probability of detection, P_D, is given by

$$P_D = \Pr\{Y_i>\gamma; Y_1,Y_2,\ldots,Y_{i-1},Y_{i+1},\ldots,Y_{M-1}\le Y_i\,|H_i\} \tag{54}$$

which, by eliminating the threshold, can be shown to be evaluated in terms of P_{FA} as

$$
\left.
\begin{aligned}
P_D = {} & \frac{1}{\sqrt{\pi}} \sqrt{\frac{G/K}{2PT/N_0 + G/K}} \int_{\eta}^{\infty} \exp\left\{ - \left(\frac{G/K}{2PT/N_0 + G/K} \right) \left(Y - \frac{PT/N_0}{\sqrt{2G/K}} \right)^2 \right\} \\
& \times \left[1 - \frac{1}{2} \operatorname{erfc} Y \right]^{K(M-2)+K-1} dY \\
& + \frac{K-1}{\sqrt{\pi}} \int_{\eta}^{\infty} \exp\left\{ -Y^2 \right\} \left[1 - \frac{1}{2} \operatorname{erfc} \left\{ \sqrt{\frac{G/K}{2PT/N_0 + G/K}} \left(Y - \frac{PT/N_0}{\sqrt{2G/K}} \right) \right\} \right] \\
& \times \left[1 - \frac{1}{2} \operatorname{erfc} Y \right]^{K(M-2)+K-2} dY \\
\eta \triangleq {} & \operatorname{erfc}^{-1} \left\{ 2 \left[1 - (1 - P_{FA})^{\frac{1}{K(M-1)}} \right] \right\}
\end{aligned}
\right\} \tag{55}
$$

For $K = 1$, i.e., the full-band squaring receiver, Eq. (55) reduces to Eq. (40a) as it should.

A further improvement in performance can be obtained by designing a receiver that attempts to remove the linear drift component of the received signal, thus enabling one to significantly reduce the size of the frequency subbands. This process, which shall be referred to as drift matching, constitutes replacing the correlating signals in Fig. 11 with ones that also contain test values of the linear drift distributed over the range corresponding to its maximum positive and negative values. The resulting drift-matching squaring receiver illustrated in Fig. 12 can now be motivated from the ALR with frequency drift (see Fig. 10), just as the subband squaring receiver was motivated by the structure of the ALR without drift (see Fig. 2). The key idea here is to select channel bandwidths, i.e., the value of K in the input lowpass rectangular filters, wide enough to encompass the signal after a linear drift component has been removed. Thus, the minimum channel bandwidth is ultimately determined by the residual quadratic and higher-order terms in the frequency trajectory. In contrast to Fig. 11, the subband no longer need include the frequency variation corresponding to the maximum linear frequency drift over the observation interval. This receiver structure is quite similar to the maximum-likelihood estimator of frequency and frequency rate described earlier in [7].

To obtain the ROC of Fig. 12, we proceed as follows. Letting J denote the number of test values of $\dot{f}$ per test value of f, then the false alarm and detection probabilities are given by Eqs. (48) and (50), respectively, with K replaced by KJ. The moments of the decision variables under the noise-only and signal-plus-noise hypotheses are still given by Eqs. (49) and (51), respectively, keeping in mind, however, that the value of K to be used in these equations is significantly larger than that previously used for the subband receiver of Fig. 11. Finally, eliminating the unknown detection threshold between Eqs. (48) and (50) results in the following ROC for the two-hypothesis case:

$$
\begin{aligned}
P_D = {} & 1 - [1 - P_{FA}]^{(KJ-1)/KJ} \\
& \times \left[1 - \frac{1}{2} \operatorname{erfc} \left\{ \sqrt{\frac{G/K}{2PT/N_0 + G/K}} \left(\operatorname{erfc}^{-1} \left(2 \left[1 - (1 - P_{FA})^{1/KJ} \right] \right) - \frac{PT/N_0}{\sqrt{2G/K}} \right) \right\} \right]
\end{aligned} \tag{56}
$$

For $J = 1$, Eq. (56) reduces to Eq. (52) as it should.

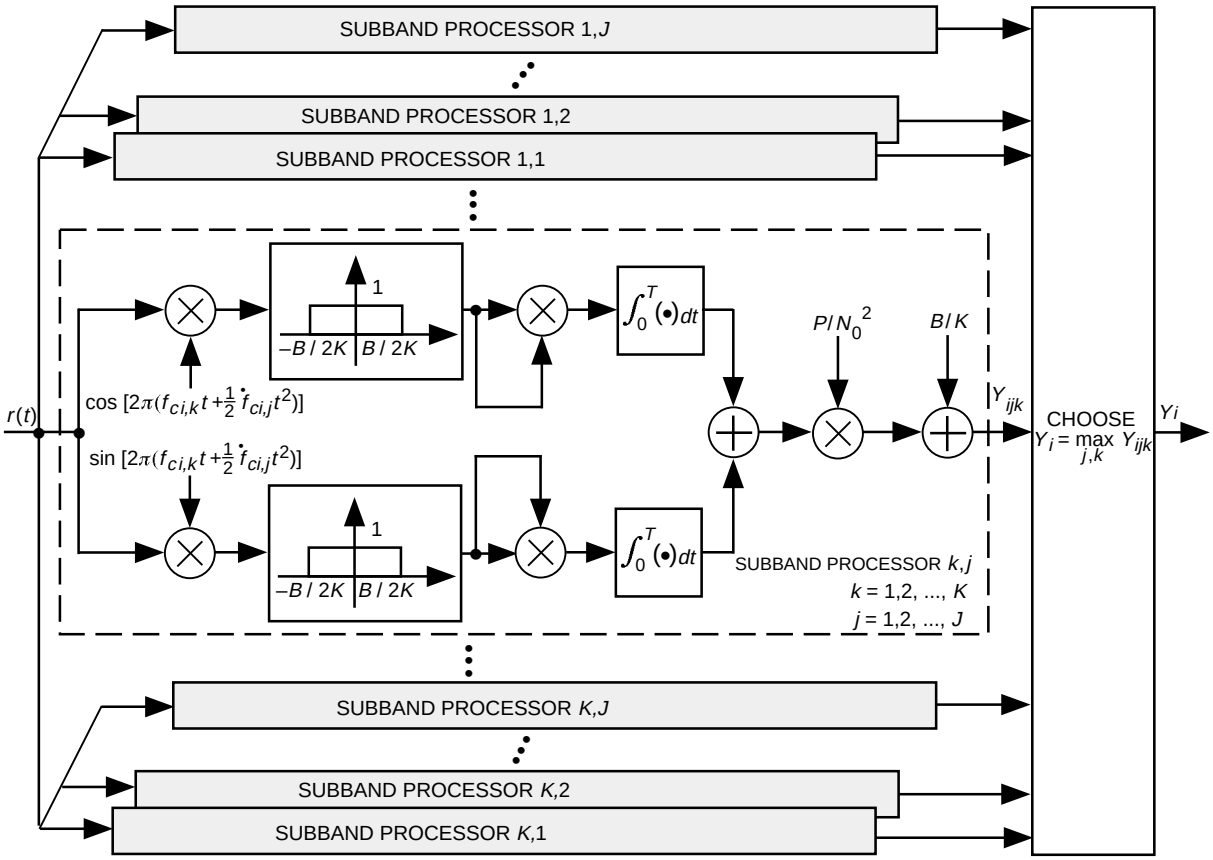

Fig. 12. The channel *i* noncoherent processor for the subband drift-matching receiver.

For the M hypothesis case, the probability of false alarm is once again given by Eq. (53) with K replaced by KJ, and the probability of detection is still given by Eq. (54). Eliminating the threshold between the two probabilities gives an ROC analogous to Eq. (55), namely,

$$\left.\begin{aligned} P_D = {} & \frac{1}{\sqrt{\pi}}\sqrt{\frac{G/K}{2PT/N_0+G/K}}\int_\eta^\infty \exp\left\{-\left(\frac{G/K}{2PT/N_0+G/K}\right)\left(Y-\frac{PT/N_0}{\sqrt{2G/K}}\right)^2\right\} \\ & \times\left[1-\frac{1}{2}\operatorname{erfc}\,Y\right]^{KJ(M-2)+KJ-1} dY \\ & + \frac{KJ-1}{\sqrt{\pi}}\int_\eta^\infty \exp\left\{-Y^2\right\}\left[1-\frac{1}{2}\operatorname{erfc}\left\{\sqrt{\frac{G/K}{2PT/N_0+G/K}}\left(Y-\frac{PT/N_0}{\sqrt{2G/K}}\right)\right\}\right] \\ & \times\left[1-\frac{1}{2}\operatorname{erfc}\,Y\right]^{KJ(M-2)+KJ-2} dY \\ \eta \triangleq {} & \operatorname{erfc}^{-1}\left\{2\left[1-(1-P_{FA})^{\frac{1}{KJ(M-1)}}\right]\right\} \end{aligned}\right\} \quad (57)$$

The performance of the receiver in Fig. 12, as described by Eqs. (56) and (57), is superimposed on the results of Fig. 9. Values of (K, J) corresponding to (500, 25), (1000, 50), and (2000, 100) were assumed to characterize the performance of the drift-matching subband squaring receiver. Difficulties in computing the large number of test statistics required for this structure prevented verification by means of computer simulations. Note that J is determined from the maximum total (positive and negative) drift $\dot{B}T$, the maximum total (positive and negative) frequency uncertainty B, and K by $J = 2K\dot{B}T/B$, where we have assumed that the subbands of width B/K within the total drift $\dot{B}T$ overlap by $B/2K$. Comparing these results with those obtained for the subband receiver of Fig. 11, we see another dramatic improvement in performance. As before, performance for $M = 5$ (four signals) is only slightly worse than for $M = 2$ (the single-tone case).

IV. Bayes (Minimum Average Cost) Test for *M* Hypotheses

As discussed in the introduction, when the a priori probabilities and costs associated with the various hypotheses are unequal, then the appropriate test to apply to the detection problem is the Bayes test, wherein the average cost (risk) is minimized. We now present a mathematical model for a Bayesian detection of M hypotheses and then derive a receiver structure that implements the resulting decision criterion.

Let C_{ij} denote the cost of deciding hypothesis H_i when in fact H_j is true. Let $P(H_j)$ denote the a priori probability of H_j. Then, the average cost is given by

$$\bar{C} = \sum_{i=0}^{M-1} \sum_{j=0}^{M-1} C_{ij} P(H_j) P(H_i | H_j) \tag{58}$$

where, as previously denoted, $P(H_i | H_j)$ is the probability of hypothesis H_i when in fact H_j is true and is defined analogously to Eq. (4) as

$$\Pr\{H_i | H_j\} = \int_{R_i} p(\mathbf{r} | H_j)\, d\mathbf{r}, \quad i, j = 1, 2, \ldots, M-1 \tag{59}$$

Following the approach in [5], we can rewrite $\bar{C}$ in the form[8]

$$\bar{C} = \sum_{i=0}^{M-1} P(H_i) C_{ii} + \sum_{i=0}^{M-1} \int_{R_i} \sum_{\substack{j=0 \\ j \neq i}}^{M-1} P(H_j)(C_{ij} - C_{jj}) p(\mathbf{r} | H_j)\, d\mathbf{r} \tag{60}$$

Defining the arguments of the integrals by

$$I_i(\mathbf{r}) \triangleq \sum_{\substack{j=0 \\ j \neq i}}^{M-1} P(H_j)(C_{ij} - C_{jj})\, p(\mathbf{r} | H_j) \tag{61}$$

then, since the first term of Eq. (60) is constant and thus independent of the decision rule, to minimize $\bar{C}$, one should

[8] Actually, VanTrees [5] writes this form only for $M = 3$. However, the extension to arbitrary M is straightforward.

$$\text{Choose the hypothesis } H_{i^*} \text{ such that } i^* = \min_i {}^{-1} I_i(\mathbf{r}) \tag{62}$$

Alternately, defining the likelihood ratios

$$\left.\begin{aligned} \Lambda_i(\mathbf{r}) &= \frac{p(\mathbf{r}\,|H_i)}{p(\mathbf{r}\,|H_0)}, \quad i = 1, 2, \ldots, M-1 \\ \Lambda_0(\mathbf{r}) &= 1 \end{aligned}\right\} \tag{63}$$

then dividing $I_i(\mathbf{r})$ by $p(\mathbf{r}\,|H_0)$ (a positive quantity), we get

$$\Omega_i(\mathbf{r}) \triangleq \frac{I_i(\mathbf{r})}{p(\mathbf{r}\,|H_0)} = \sum_{\substack{j=0 \\ j\neq i}}^{M-1} \overbrace{P(H_j)(C_{ij} - C_{jj})}^{w_{ij}} \Lambda_j(\mathbf{r}), \quad i = 1, 2, \ldots, M-1 \tag{64}$$

which results in the equivalent decision rule:

$$\text{Choose the hypothesis } H_{i^*} \text{ such that } i^* = \min_i {}^{-1} \Omega_i(\mathbf{r}) \tag{65}$$

Note that Eq. (64), which represents the transformation from the likelihood functions to the decision variables, is a linear weighting and can thus be written in matrix form as

$$\boldsymbol{\Omega} = W\boldsymbol{\Lambda} \tag{66}$$

where

$$\left.\begin{aligned} \boldsymbol{\Omega} &= \left[\Omega_0(\mathbf{r}), \Omega_1(\mathbf{r}), \Omega_2(\mathbf{r}), \ldots, \Omega_{M-1}(\mathbf{r})\right]^T \\ \boldsymbol{\Lambda} &= \left[1, \Lambda_1(\mathbf{r}), \Lambda_2(\mathbf{r}), \ldots, \Lambda_{M-1}(\mathbf{r})\right]^T \end{aligned}\right\} \tag{67}$$

and the weighting matrix W is given by

$$\left.\begin{aligned} W &= \{w_{ij}\} \\ w_{ii} &= 0 \\ w_{ij} &= P(H_i)(C_{ij} - C_{ii}) \end{aligned}\right\} \tag{68}$$

i.e., a square $M \times M$ matrix with zeros along the diagonal. Quite often the cost of making a correct decision is assumed to be zero and, thus, the off-diagonal weights in Eq. (68) simplify to

$$w_{ij} = P(H_i)\, C_{ij} \tag{69}$$

For the M-hypothesis testing problem under consideration in this article, the likelihood ratios defined in Eq. (63) have already been computed previously [1]. For example, for a set of $M-1$ sinusoidal signals with unknown phase and known frequency (as investigated in Section III.A.2),

$$\left.\begin{aligned} \Lambda_i(\mathbf{r}) &= \Lambda_i(r(t)) = \exp\left(-\frac{PT}{N_0}\right) I_0\left(\frac{2\sqrt{P}}{N_0} L_{ci}\right), \quad i = 1, 2, \ldots, M-1 \\ \Lambda_0(\mathbf{r}) &= \Lambda_0(r(t)) = 1 \end{aligned}\right\} \tag{70}$$

where the envelope L_{ci} is defined in Eq. (12). Using Eq. (66) in Eq. (64) together with Decision Rule (65) suggests the receiver illustrated in Fig. 13.

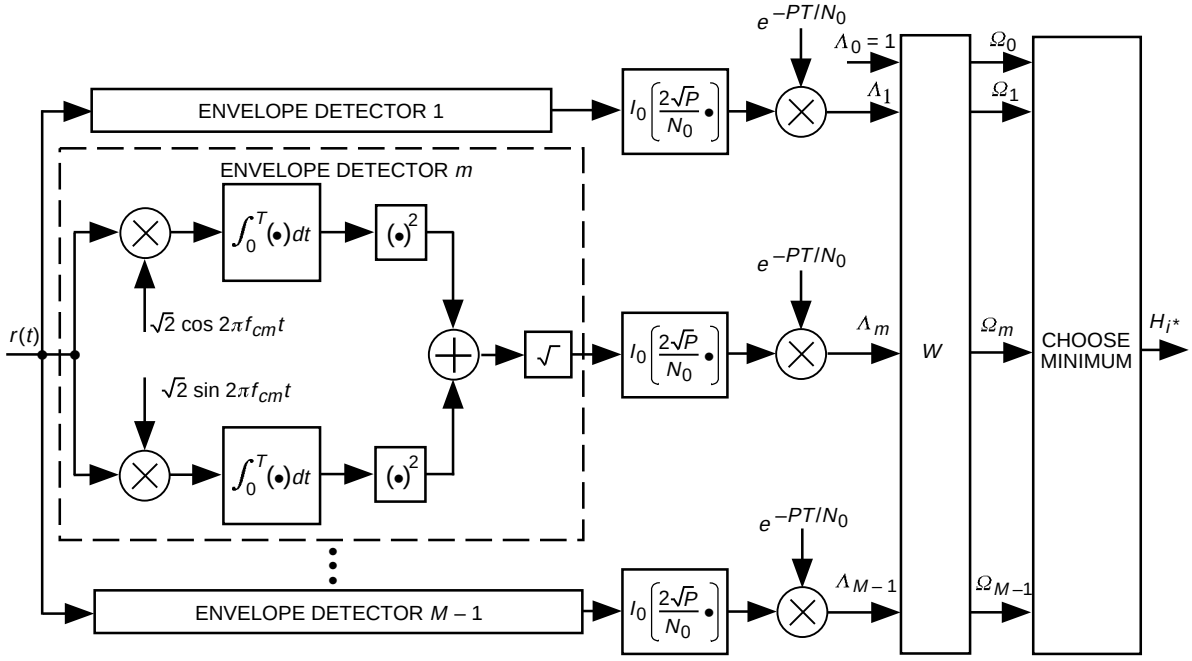

Fig. 13. The Bayesian detector for detection of $M-1$ sinusoidal tones with unknown phase and known frequency in AWGN.

References

[1] M. K. Simon, M. M. Shihabi, and T. Moon, "Optimum Detection of Tones Transmitted by a Spacecraft," *The Telecommunications and Data Acquisition Progress Report 42-123, July–September 1995*, Jet Propulsion Laboratory, Pasadena, California, pp. 69–98, November 15, 1995.
http://tda.jpl.nasa.gov/tda/progress_report/42-123/123A.pdf

[2] T. Kailath, "General Likelihood-Ratio Formula for Random Signals in Gaussian Noise," *IEEE Transactions on Information Theory*, vol. IT-15, no. 3, pp. 350–361, May 1969.

[3] W. C. Lindsey and M. K. Simon, *Telecommunication Systems Engineering*, Englewood Cliffs, New Jersey: Prentice-Hall, Inc., 1973, reprinted by Dover Press, New York, 1994.

[4] A. D. Whalen, *Detection of Signals in Noise*, New York: Academic Press, 1971.

[5] H. L. VanTrees, *Detection, Estimation, and Modulation Theory, Part III*, New York: John Wiley & Sons, pp. 46–49, 1968.

[6] M. Abramowitz and I. A. Stegun, *Handbook of Mathematical Functions*, National Bureau of Standards Applied Mathematics Series 55, Washington, DC: U.S. Department of Commerce, 1964.

[7] V. A. Vilnrotter, S. Hinedi, and R. Kumar, "Frequency Estimation Techniques for High Dynamic Trajectories," *IEEE Transactions on Aerospace and Electronic Systems*, vol. 25, no. 4, pp. 559–577, July 1989.

Appendix A

On the Estimator–Correlator Representation of Average-Likelihood Ratios

I. Introduction

In the study of detection problems involving signals (deterministic or random) corrupted by additive Gaussian noise, it is well-known that a likelihood ratio test is optimum in the sense of maximizing the probability of detection P_D for a given false alarm probability P_{FA} (the so-called Neyman–Pearson criterion). When the randomness of the signal is in the form of one or more unknown parameters, e.g., a sinusoidal carrier with unknown phase, frequency, etc., then the likelihood ratio mentioned above is obtained by statistically averaging over the unknown parameters, which implies knowledge of their probability density functions (pdf's), resulting in a so-called average-likelihood ratio test. Receiver structures based on such average-likelihood ratio tests for various signals of practical interest are well documented in the literature and result in optimum detection performance in accordance with the above definition of optimality.

It is often intuitively satisfying to view the average-likelihood ratio mentioned above in the form of an estimator–correlator processor. In particular, one first estimates the random signal, $s(t)$, and then correlates this estimated signal, $\hat{s}(t)$, with the received signal, $r(t)$, over the duration of the observation, T. The average-likelihood ratio (actually the natural logarithm of this ratio) is then obtained by subtracting from this correlation $\int_0^T r(t)\hat{s}(t)dt$, an appropriate bias term proportional to the energy in the signal estimate, i.e., $(1/2)\int_0^T \hat{s}^2(t)dt$. The equivalence between the traditional form of the average-likelihood ratio (namely, the ratio of the pdf's of $r(t)$ under the two-hypothesis signal present (H_1) and signal absent (H_0)) and the estimator–correlator form was established many years ago by Kailath [2]. In particular, he showed that the appropriate signal estimator to use for $\hat{s}(t)$ was the conditional mean of $r(t)$, given observations up to the instant t and assuming the signal-present hypothesis (H_1). It is important to emphasize at this point that the traditional and the estimator–correlator forms of the average-likelihood ratio are exactly equivalent (and thus would produce identical receiver performances.)

The primary motivation for introducing the estimator–correlator philosophy is to allow engineering approximations of this form of optimum receiver with other, perhaps simpler to implement, signal estimators. With rare exceptions, such approximate estimator–correlator receivers will yield suboptimum performance relative to the true average-likelihood structure.[1]

In the case where the signal randomness is described by a vector of unknown parameters (such as the sinusoidal carrier with unknown phase, frequency, etc.), it is tempting to use for the estimate of the signal a sinusoidal carrier whose phase, frequency, etc., are replaced by the maximum-likelihood estimates of these random parameters. These maximum-likelihood estimates are obtained from suitable processing of the received signal over the entire observation interval of T s and, thus, differ considerably from the optimum conditional mean estimator described above, which is obtained as a continuous function of time t throughout the observation interval. It is to be emphasized that such a form of signal estimator when used with an estimator–correlator structure will *never result in the true average-likelihood ratio.* What is interesting, *and strictly a coincidence*, is the fact that for the case of a sinusoidal carrier with known frequency but unknown (random) phase [assumed to be uniformly distributed in the interval $(-\pi, \pi)$], an estimator–correlator using as a signal estimate the same sinusoidal carrier with a phase equal to

[1] *At best*, these other estimator–correlator structures based upon signal estimators other than the specific one described above will perform equally to the true optimum structure.

the maximum-likelihood estimate of phase, $\hat{\theta}_{ML}$, results in optimum receiver performance. That is, even though this approximate estimator–correlator structure does not achieve the true average-likelihood ratio, it does result in an equivalent average-likelihood ratio test, i.e., a comparison of the likelihood ratio with a threshold determined from the given false alarm probability. It is to be emphasized again that this is strictly a coincidence, and one should not mislead oneself into thinking that it can be extended to the case where other signal parameters are unknown. For example, if *both* signal carrier phase and frequency are unknown and random, then an estimator–correlator structure using as a signal estimator this same carrier with phase and frequency equal to the maximum-likelihood estimates of these parameters *produces neither the true average-likelihood ratio nor an equivalent average-likelihood ratio test.* More specifically, such an approximate estimator–correlator structure will have suboptimum performance relative to that based on the true average-likelihood ratio.

At this point, we turn to a mathematical formulation of some of the above statements, using as examples the case where the signal is a sinusoidal carrier with unknown phase and frequency parameters.

II. Mathematical Model

We begin by considering the following canonical detection problem. Given an observation $\{r(t), 0 \leq t \leq T \leq \infty\}$, determine which of the following hypotheses is true:

$$\left.\begin{array}{ll} H_1: & r(t) = s(t) + n(t) \\ H_0: & r(t) = n(t) \end{array}\right\} \tag{A-1}$$

where $s(t)$ denotes the signal (deterministic or random) and $n(t)$ denotes the additive white Gaussian noise.[2] The traditional likelihood function approach is to compute the likelihood ratio (LR), Λ, namely,

$$\Lambda \triangleq \frac{p\left(r(t)\,|H_1\right)}{p\left(r(t)\,|H_0\right)} \tag{A-2}$$

and compare this quantity to a threshold, γ, resulting in the likelihood ratio test

$$\Lambda \underset{H_0}{\overset{H_1}{\gtrless}} \gamma \tag{A-3}$$

In [2], it is shown that the LR defined in Eq. (A-2) can be expressed in a form that implies an estimator–correlator type of detector, namely,

$$\Lambda = \exp\left\{\int_0^T r(t)\hat{s}(t)dt - \frac{1}{2}\int_0^T \hat{s}^2(t)dt\right\} \tag{A-4}$$

where

[2] For our purposes, the additive noise will be taken to be white Gaussian although the formulation given in [1] allows for a much more general statistical noise model.

$$\hat{s}(t) \triangleq E\left\{r(\tau)\,|\tau \le t, H_1\right\} \tag{A-5}$$

It is well-known that $\hat{s}(t)$ is the least-squares estimate (not necessarily linear) of $s(t)$ given noisy data $\{s(\tau)+n(\tau), \tau < t\}$ up to time t. If H_1 is not the true hypothesis, then $\hat{s}(t)$ of Eq. (A-5) is not the least-squares estimate of $s(t)$; it may be called a pseudoestimate of $s(t)$.

Since the natural logarithm is a monotonic function of its argument, then an equivalent LR test to Eq. (A-3) is

$$\lambda \underset{H_0}{\overset{H_1}{\gtrless}} \gamma \qquad \gamma \triangleq \ln \Gamma, \qquad \lambda \triangleq \ln \Lambda \tag{A-6}$$

or using Eq. (A-4),

$$\int_0^T r(t)\hat{s}(t)dt - \frac{1}{2}\int_0^T \hat{s}^2(t)dt \underset{H_0}{\overset{H_1}{\gtrless}} \gamma \tag{A-7a}$$

or equivalently,

$$\int_0^T r(t)\hat{s}(t)dt \underset{H_0}{\overset{H_1}{\gtrless}} \gamma' \tag{A-7b}$$

where the energy term has been combined with the original threshold γ to form a new threshold γ'. Figure A-1 is a graphical illustration of Eq. (A-7b). The specific implementation of the block labeled signal estimation depends on the statistical characterization of the signal $s(t)$. We shall illustrate this evaluation for two cases of interest, namely, $s(t)$ equal to a sinusoidal carrier with known frequency and unknown phase, and $s(t)$ equal to a sinusoidal carrier with unknown frequency and unknown phase. In both cases, the signal amplitude (which may be time varying over the observation) is assumed to be known. Before proceeding with these specific evaluations, we first derive an expression for the estimator of Eq. (A-5) that is valid for an arbitrary characterization of $s(t)$.

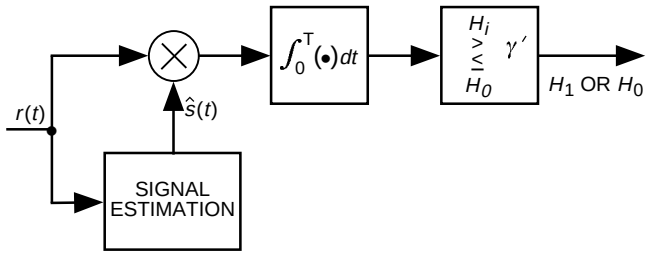

Fig. A-1. The estimator–correlator form of the optimum receiver.

By definition, the conditional mean specified in Eq. (A-5) is given by

$$\hat{s}(t) \triangleq \int s(t) p\left(s(t)\,|r(\tau); \tau \le t\,\right) ds(t) \tag{A-8}$$

where $r(\tau) = s(\tau) + n(\tau)$. Using Bayes' rule, namely,

$$p\left(s(t)\,|r(\tau); \tau \le t\,\right) = \frac{p\left(r(\tau); \tau \le t\,|s(t)\,\right) p\left(s(t)\right)}{p\left(r(\tau); \tau \le t\right)}$$

$$= \frac{p\left(r(\tau); \tau \le t\,|s(t)\,\right) p\left(s(t)\right)}{\int p\left(r(\tau); \tau \le t\,|s(t)\,\right) p\left(s(t)\right) ds(t)} \tag{A-9}$$

we can rewrite Eq. (A-8) as

$$\hat{s}(t) \triangleq \frac{\int s(t) p\left(r(\tau), \tau \le t\,|s(t)\,\right) p\left(s(t)\right) ds(t)}{\int p\left(r(\tau), \tau \le t\,|s(t)\,\right) p\left(s(t)\right) ds(t)} \tag{A-10}$$

A. Sinusoidal Signal With Known Frequency and Unknown Phase

Consider a signal of the form

$$s(t) = A(t) \cos\left(\omega t + \theta\right) \tag{A-11}$$

where $A(t)$ is a known deterministic signal amplitude that is "slowly varying" compared with the known frequency ω, and θ is a random phase assumed to be uniformly distributed in the interval $(-\pi, \pi)$. Note that since θ is constant (with time) over the duration of the observation, then conditioning on $s(t)$ in Eq. (A-10) is equivalent to conditioning on θ, which in turn implies conditioning on $s(t)$ for all the past, i.e., $s(t), \tau \le t$. Thus,

$$p\left(r(\tau), \tau \le t\,|s(t)\,\right) = p\left(r(\tau), \tau \le t\,|s(\tau), \tau \le t\,\right) \tag{A-12}$$

Since our observation interval is assumed to be $(0, T)$, then for our purposes, the infinite past $\tau \le t$ can be replaced by $0 \le \tau \le t$. Since $r(t)$ corresponds to the addition of white Gaussian noise, $n(t)$, to the signal in Eq. (A-11), then using Eq. (A-12), we get

$$p\left(r(\tau), \tau \le t\,|s(t)\,\right) = C \exp\left(-\frac{1}{N_0} \int_0^t \left(r(\tau) - s(\tau)\right)^2 d\tau\right)$$

$$= C \exp\left(-\frac{1}{N_0} \int_0^t r^2(\tau) d\tau\right) \exp\left(\frac{2}{N_0} \int_0^t r(\tau) s(\tau) d\tau\right) \exp\left(-\frac{1}{N_0} \int_0^t s^2(\tau) d\tau\right) \tag{A-13}$$

where N_0 is the single-sided noise spectral density in W/Hz. The first of the three exponential terms in Eq. (A-13) is independent of the signal $s(t)$ and thus will cancel when used in both the numerator and denominator of Eq. (A-10). The third exponential term of Eq. (A-13) approximately (for the assumed slow variation of $A(t)$) evaluates to

$$\exp\left(-\frac{1}{N_0}\int_0^t s^2(\tau)d\tau\right) \cong \exp\left(-\frac{\int_0^t A^2(\tau)d\tau}{2N_0}\right) \tag{A-14}$$

which again will be common to both the numerator and denominator of Eq. (A-10) and hence will also cancel. Finally, the middle exponential term of Eq. (A-13) becomes

$$\begin{aligned}\exp\left(\frac{2}{N_0}\int_0^t r(\tau)s(\tau)d\tau\right) &= \exp\left(\frac{2}{N_0}\left[\cos\theta\int_0^t r(\tau)A(\tau)\cos\omega\tau d\tau - \sin\theta\int_0^t r(\tau)A(\tau)\sin\omega\tau d\tau\right]\right) \\ &= \exp\left\{V(t)\cos\left(\theta-\phi(t)\right)\right\}\end{aligned} \tag{A-15}$$

where

$$\left.\begin{aligned} V_c(t) &\triangleq \int_0^t r(\tau)A(\tau)\cos\omega\tau d\tau \\ V_s(t) &\triangleq \int_0^t r(\tau)A(\tau)\sin\omega\tau d\tau \\ V(t) &\triangleq \sqrt{V_c^2(t)+V_s^2(t)} \\ \phi(t) &\triangleq -\tan^{-1}\frac{V_s(t)}{V_c(t)} \end{aligned}\right\} \tag{A-16}$$

Since $p(s(t))ds(t) = p_\theta(\theta)d\theta$, then in view of the above, the denominator of Eq. (A-10) becomes

$$\int p\left(r(\tau), \tau \le t\,|s(t)\right)p\left(s(t)\right)ds(t) = C'(t)\int \exp\left\{V(t)\cos\left(\theta-\phi(t)\right)\right\}p(\theta)d\theta \tag{A-17}$$

where $C'(t)$ includes the first and third exponential terms of Eq. (A-13). Averaging over the uniform distribution of θ, i.e., $p(\theta) = 1/2\pi, -\pi \le \theta \le \pi$, we get the final result

$$\int p\left(r(\tau), \tau \le t\,|s(t)\right)p\left(s(t)\right)ds(t) = C'(t)I_0\left(V(t)\right) \tag{A-18}$$

where $I_0(x)$ is the modified zero-order Bessel function of the first kind with argument x. Similarly, the numerator of Eq. (A-10) evaluates to

$$\int s(t)p\left(r(\tau), \tau \le t\,|s(t)\right)p\left(s(t)\right)ds(t) = C'(t)\int A(t)\cos\left(\omega t+\theta\right)\exp\left\{V(t)\cos\left(\theta-\phi(t)\right)\right\}p(\theta)d\theta \tag{A-19}$$

Again employing the uniform distribution on θ, we get

$$C'(t)\int A(t)\cos(\omega t+\theta)\exp\{V(t)\cos(\theta-\phi(t))\}\,p(\theta)d\theta =$$

$$C'(t)A(t)\cos(\omega t+\phi(t))\overbrace{\frac{1}{2\pi}\int_{-\pi}^{\pi}\cos(\theta-\phi(t))\exp\{V(t)\cos(\theta-\phi(t))\}\,d\theta}^{=I_1(V(t))}$$

$$-C'(t)A(t)\sin(\omega t+\phi(t))\underbrace{\frac{1}{2\pi}\int_{-\pi}^{\pi}\sin(\theta-\phi(t))\exp\{V(t)\cos(\theta-\phi(t))\}\,d\theta}_{=0} \qquad \text{(A-20)}$$

Finally, then,

$$\int s(t)p\left(r(\tau),\tau\le t\,|s(t)\right)p\left(s(t)\right)ds(t) = C'(t)A(t)\cos(\omega t+\phi(t))\,I_1\left(V(t)\right) \qquad \text{(A-21)}$$

where $I_1(x)$ is the modified first-order Bessel function of the first kind with argument x. Taking the ratio of Eq. (A-18) to Eq. (A-21) gives the signal estimator in accordance with Eq. (A-10), namely,

$$\hat{s}(t) = A(t)\frac{I_1\left(V(t)\right)}{I_0\left(V(t)\right)}\cos(\omega t+\phi(t)) \qquad \text{(A-22)}$$

An illustration of the implementation of $\hat{s}(t)$ in Eq. (A-22) integrated into the estimator–correlator receiver is illustrated in Fig. A-2.

If, instead of the estimator–correlator, one were to use the traditional average-likelihood function approach as described by Eq. (A-2), then for the case at hand, Eq. (A-2) would become

$$\Lambda \triangleq \frac{\int_{-\pi}^{\pi} p\left(r(t)\,|H_1,\theta\right)p(\theta)d\theta}{p\left(r(t)\,|H_0,\theta\right)} \qquad \text{(A-23)}$$

which for the uniform distribution on θ and the signal of Eq. (A-11) gives the well-known result (see [1] for example)

$$\lambda = \ln\Lambda = \ln I_0\left(V(T)\right) - \frac{1}{4}\int_0^T A^2(t)dt \qquad \text{(A-24)}$$

When the second term in Eq. (A-24) is absorbed into the detection threshold, we obtain the classical noncoherent detector illustrated in Fig. A-3, which is based on the LR test

$$\ln I_0\left(V(T)\right) \underset{H_0}{\overset{H_1}{\gtrless}} \gamma'' \qquad \gamma'' = \gamma + \frac{1}{4}\int_0^T A^2(t)dt \qquad \text{(A-25)}$$

Clearly, the receiver of Fig. A-3(a), obtained by averaging out the phase in the numerator of the likelihood ratio, is less complex than its estimator–correlator counterpart of Fig. A-2 and is, thus, the preferred

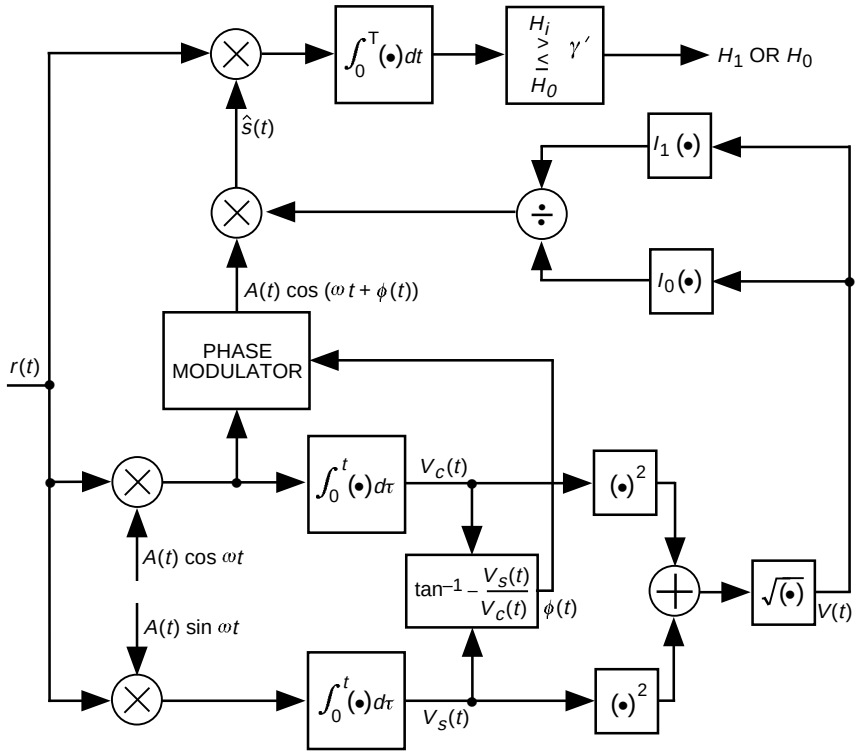

Fig. A-2. The estimator–correlator form of the optimum receiver with signal estimator for a sinusoidal carrier with known frequency and unknown phase.

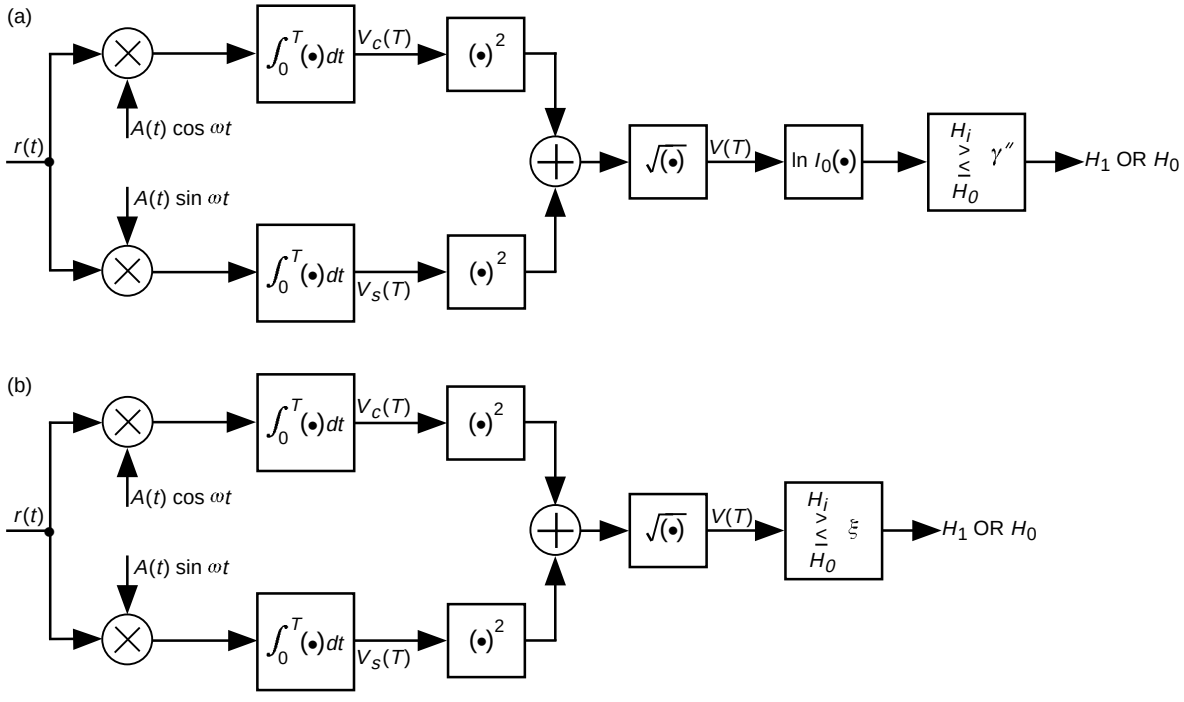

Fig. A-3. Noncoherent detectors for a sinusoidal carrier with known frequency and unknown phase: (a) obtained by averaging out the phase in the numerator of the likelihood ratio and (b) a further simplified alternate form.

implementation. In fact, in terms of a likelihood ratio test, Fig. A-3(a) can be further simplified to Fig. A-3(b) by noting that the $\ln I_0(x)$ function is monotonic in its argument x, and thus Eq. (A-25) can be rewritten as

$$V(T) \underset{H_0}{\overset{H_1}{\gtrless}} \xi \tag{A-26}$$

where ξ is yet another normalized threshold.

For the signal in Eq. (A-11), the maximum-likelihood estimate of θ based on the entire observation interval $0 \le t \le T$ is given by $\hat{\theta}_{ML} = \phi(T)$, where $\phi(t)$ is defined in Eq. (A-16). This is easily seen from Eq. (A-15) by noting that, for $t = T$, the exponential is maximized by making the argument of the cosine function equal to zero. Replacing θ by $\hat{\theta}_{ML}$ in Eq. (A-11) and using this result as an estimate of the signal in the estimator–correlator structure of Fig. A-1 results in the following correlator output:

$$\begin{aligned}
\int_0^T r(t)\hat{s}(t)dt &= \int_0^T r(t)A(t)\cos\left(\omega t + \hat{\theta}_{ML}\right)dt \\
&= \cos\hat{\theta}_{ML}\overbrace{\int_0^T r(t)A(t)\cos\omega t dt}^{V_c(T)} - \sin\hat{\theta}_{ML}\overbrace{\int_0^T r(t)A(t)\sin\omega t dt}^{V_s(T)} \\
&= \frac{V_c(T)}{V(T)}V_c(T) - \frac{-V_s(T)}{V(T)}V_s(T) = \frac{V_c^2(T)+V_s^2(T)}{V(T)} = V(T)
\end{aligned} \tag{A-27}$$

Thus, although the correlator output is not equal to the average-likelihood *ratio* as in Eq. (A-25), in view of Eq. (A-26), it does, however, result in an optimum-likelihood *test*. This receiver structure is illustrated in Fig. A-4.

B. Sinusoidal Signal With Unknown Frequency and Unknown Phase

Consider a signal of the form in Eq. (A-11) where now the frequency $f = \omega/2\pi$ is also unknown and assumed to be uniformly distributed in the interval $(f_c - B/2, f_c + B/2)$. Again, since θ and f are constant (with time) over the duration of the observation, then conditioning on $s(t)$ in Eq. (A-10) is equivalent to conditioning on θ and f, which in turn implies conditioning on $s(t)$ for all the past, i.e., $s(t), \tau \le t$, as in Eq. (A-12). Proceeding as before, we arrive at an expression identical to Eq. (A-18), which we now express as

$$\begin{aligned}
\exp\left(\frac{2}{N_0}\int_0^t r(\tau)s(\tau)d\tau\right) &= \exp\left(\frac{2}{N_0}\left[\cos\theta\int_0^t r(\tau)A(\tau)\cos 2\pi f\tau d\tau - \sin\theta\int_0^t r(\tau)A(\tau)\sin 2\pi f\tau d\tau\right]\right) \\
&= \exp\left\{V(t,f)\cos\left(\theta - \phi(t,f)\right)\right\}
\end{aligned} \tag{A-28}$$

where

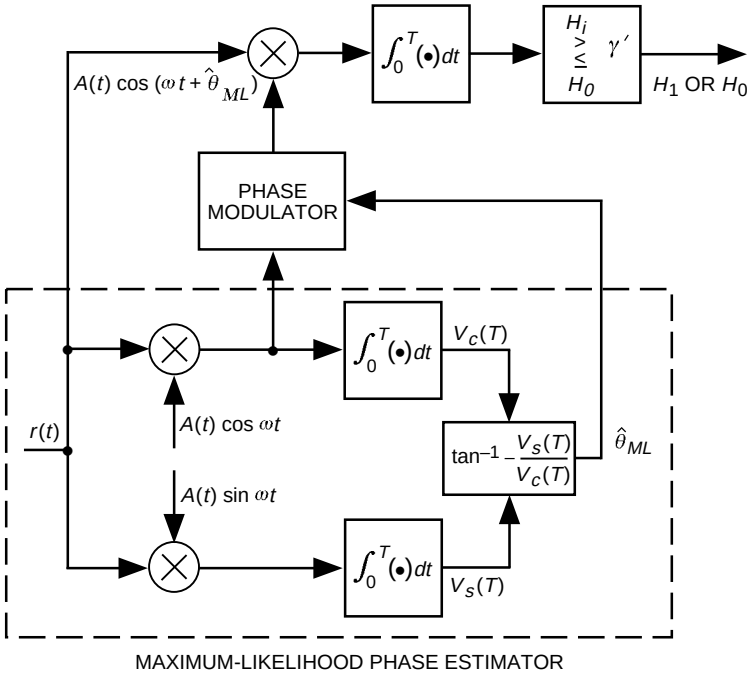

Fig. A-4. The maximum-likelihood phase estimator and pseudocoherent detector of a sinusoidal carrier with known frequency and unknown phase.

$$\left.\begin{aligned} V_c(t,f) &\triangleq \int_0^t r(\tau)A(\tau)\cos 2\pi f\tau d\tau \\ V_s(t,f) &\triangleq \int_0^t r(\tau)A(\tau)\sin 2\pi f\tau d\tau \\ V(t,f) &\triangleq \sqrt{V_c^2(t,f)+V_s^2(t,f)} \\ \phi(t,f) &\triangleq -\tan^{-1}\frac{V_s(t,f)}{V_c(t,f)} \end{aligned}\right\} \tag{A-29}$$

and we have specifically introduced into the notation the dependence on the unknown parameter f. First averaging over the unknown phase as before and then over the unknown frequency gives [analogously to Eq. (A-18)]

$$\int p\left(r(\tau),\tau\le t\,|s(t)\,\right)p\left(s(t)\right)ds(t) = C'(t)\frac{1}{B}\int_{f_c-B/2}^{f_c+B/2} I_0\left(V(t,f)\right)df \tag{A-30}$$

Similarly, the numerator of Eq. (A-10) evaluates to

$$\int p\left(r(\tau),\tau\le t\,|s(t)\,\right)p\left(s(t)\right)ds(t) = C'(t)A(t)\frac{1}{B}\int_{f_c-B/2}^{f_c+B/2} \cos\left(2\pi ft+\phi(t,f)\right)I_1\left(V(t,f)\right)df \tag{A-31}$$

Taking the ratio of Eq. (A-30) to Eq. (A-31) gives the signal estimator in accordance with Eq. (A-10), namely,

$$\hat{s}(t) = A(t)\frac{\int_{f_c-B/2}^{f_c+B/2} \cos\left(2\pi f t + \phi(t,f)\right) I_1\left(V(t,f)\right) df}{\int_{f_c-B/2}^{f_c+B/2} I_0\left(V(t,f)\right) df} \tag{A-32}$$

The estimator in Eq. (A-32) can be approximated by replacing the continuous integrations over f by discrete sums evaluated at frequencies separated by $1/T$, resulting in a bank of $G = BT$ correlators (see Fig. A-5).

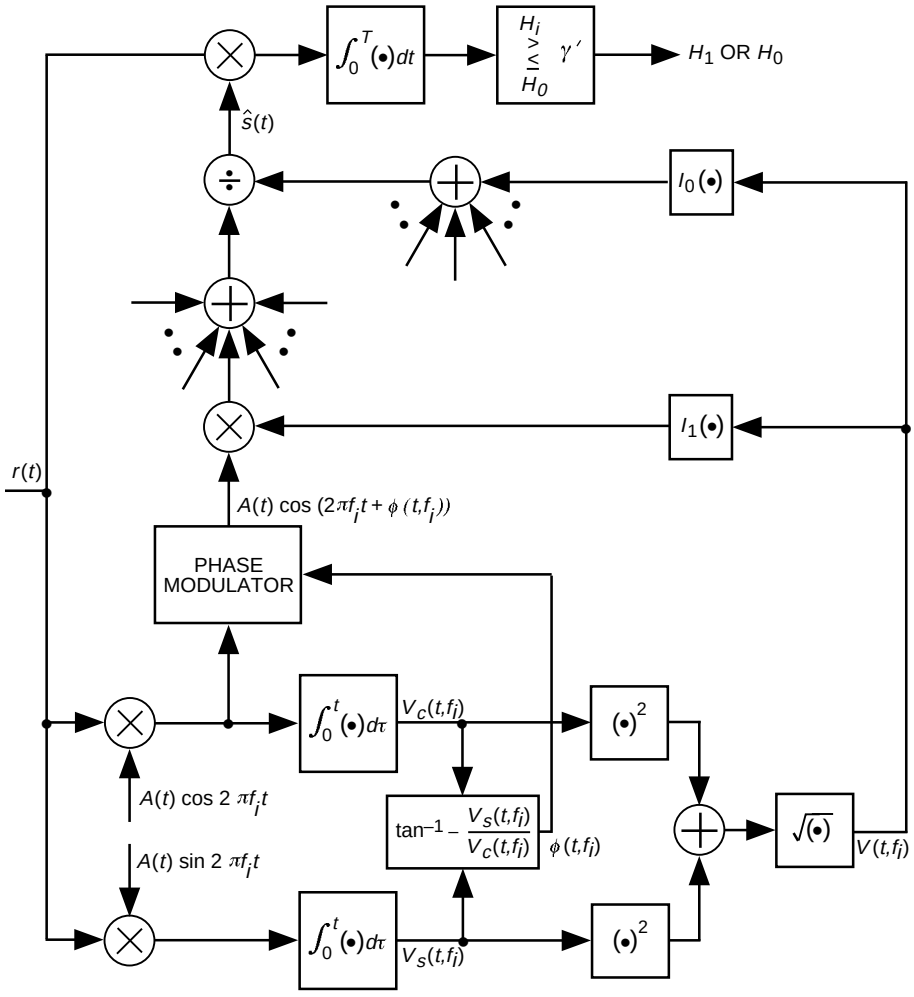

Fig. A-5. The estimator–correlator form of the optimum receiver with signal estimator for a sinusoidal carrier with unknown frequency and unknown phase.

If, instead of the estimator–correlator, one were to use the traditional average-likelihood function approach as described by Eq. (A-2), then for the case at hand, Eq. (A-2) would become

$$\Lambda \triangleq \frac{\int_{f_c-B/2}^{f_c+B/2} \int_{-\pi}^{\pi} p\left(r(t)\,|H_1, \theta\right) p(\theta) p(f) d\theta df}{p\left(r(t)\,|H_0, \theta\right)} \tag{A-33}$$

which, for the uniform distributions on θ and f and the signal of Eq. (A-11), gives the result [1]

$$\lambda = \ln \Lambda = \ln \left[\frac{1}{B} \int_{f_c-B/2}^{f_c+B/2} I_0\left(V(T,f)\right) df \right] - \frac{1}{4} \int_0^T A^2(t) dt \tag{A-34}$$

which again can be approximated with a bank of $G = BT$ correlators.

In terms of a likelihood ratio test, the logarithm in Eq. (A-34) can be ignored (since it is a monotonic of its argument); however, the Bessel function nonlinearity cannot. Also, as before, the second term in Eq. (A-34) can be absorbed into the detection threshold. The resulting structure is illustrated in Fig. A-6.

Finally, we point out that replacing θ and f by their maximum-likelihood estimates $\hat{\theta}_{ML}$ and $\hat{f}_{ML}$ and using the result as a signal estimator in the estimator–correlator structure of Fig. A-1 results neither in the average-likelihood *ratio* nor an equivalent-likelihood ratio *test*.

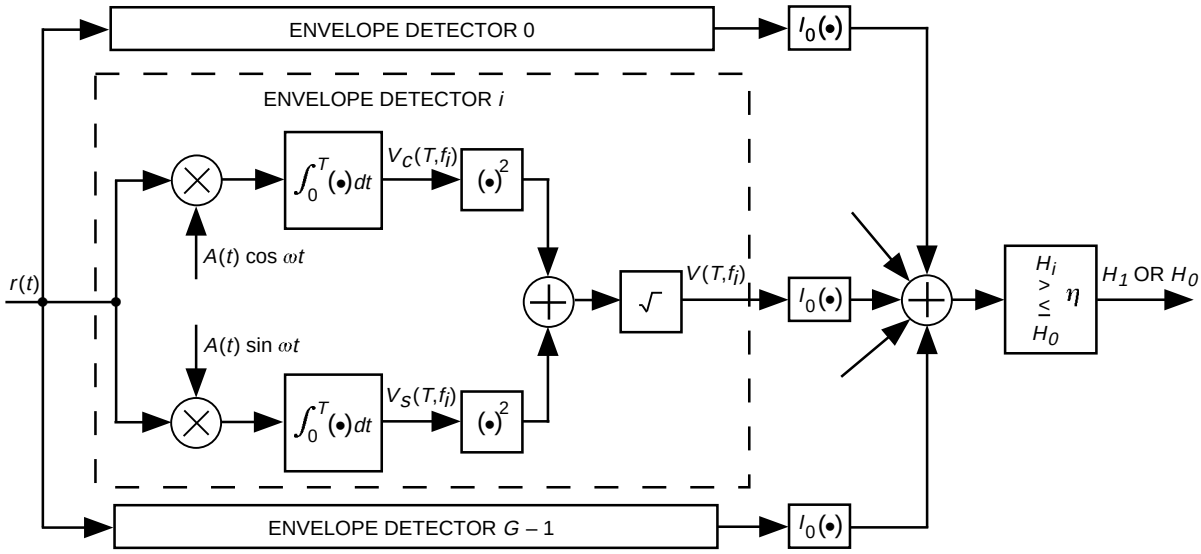

Fig. A-6. The average-likelihood (noncoherent) detector for detection of a sinusoidal tone with unknown frequency and unknown phase.

Appendix B

On the Orthogonality of a Set of Subcarrier Modulated Sinusoidal Carriers

Consider a signaling set generated by product modulating a fixed sinusoidal carrier with a set of subcarriers. In mathematical terms, the signals are characterized by[1]

$$s_i(t) = A\sin(\omega_c t + \theta_c)\sin(\omega_{sc_i} t + \theta_{sc_i})$$

$$= \frac{A}{2}\cos\left(\left(\overbrace{\omega_c + \omega_{sc_i}}^{\omega_i^+}\right)t + \overbrace{\theta_c + \theta_{sc_i}}^{\theta_i^+}\right) + \frac{A}{2}\cos\left(\left(\overbrace{\omega_c - \omega_{sc_i}}^{\omega_i^-}\right)t + \overbrace{\theta_c - \theta_{sc_i}}^{\theta_i^-}\right), \quad i = 1, 2, \ldots, M-1 \tag{B-1}$$

It was shown in [1] that for any i, θ_i^+ and θ_i^- (reduced modulo 2π) are independent when θ_c and θ_{sc_i} are independent and each uniformly distributed in $(-\pi, \pi)$. Consider the signal correlation $\int_0^T s_i(t)s_j(t)dt$, which, using Eq. (B-1), becomes

$$\begin{aligned}\int_0^T s_i(t)s_j(t)dt = \frac{A^2}{4}\Bigg[&\int_0^T \cos\left(\omega_i^+ t + \theta_i^+\right)\cos\left(\omega_j^+ t + \theta_j^+\right)dt \\ &+ \int_0^T \cos\left(\omega_i^+ t + \theta_i^+\right)\cos\left(\omega_j^- t + \theta_j^-\right)dt \\ &+ \int_0^T \cos\left(\omega_i^- t + \theta_i^-\right)\cos\left(\omega_j^+ t + \theta_j^+\right)dt \\ &+ \int_0^T \cos\left(\omega_i^- t + \theta_i^-\right)\cos\left(\omega_j^- t + \theta_j^-\right)dt\Bigg]\end{aligned} \tag{B-2}$$

Ignoring the sum frequency terms, we get

[1] In reality, the subcarriers would be square waves. However, since we only consider the first upper and lower side bands of the modulated carrier, we can equivalently consider sinusoidal subcarriers.

$$\int_0^T s_i(t)s_j(t)dt = \frac{A^2}{8}\left[\int_0^T \cos\left(\left(\omega_{sc_i} - \omega_{sc_j}\right)t + \theta_i^+ - \theta_j^+\right)dt\right.$$

$$+ \int_0^T \cos\left(\left(\omega_{sc_i} + \omega_{sc_j}\right)t + \theta_i^+ + \theta_j^-\right)dt$$

$$+ \int_0^T \cos\left(\left(-\omega_{sc_i} - \omega_{sc_j}\right)t + \theta_i^- - \theta_j^+\right)dt$$

$$\left. + \int_0^T \cos\left(\left(-\omega_{sc_i} + \omega_{sc_j}\right)t + \theta_i^- - \theta_j^-\right)dt\right] \qquad \text{(B-3)}$$

Thus, if the spacing between subcarrier frequencies is an integer multiple of the reciprocal of the observation time, i.e., $f_{sc_i} - f_{sc_j} = m/T$, then the first and fourth terms in Eq. (B-3) are zero. Furthermore, if $f_{sc_i} + f_{sc_j} >> 1/T$ for all i and j, as is typically the case, then the second and third terms of Eq. (B-3) are also zero, in which case the signaling set is orthogonal.

Appendix C
Computer Simulation Using the DETECT.FOR Program

All simulations started by generating Gaussian random samples at the output of the integrate-and-dump device (for the ALR and MLR detectors) or at the output of the lowpass filter (for the subband receiver) using theoretically computed mean and standard deviation values. These samples were then processed as required by each particular algorithm, and the output statistics were computed and checked, when possible, against the theoretical predictions. When the simulation required generating samples for extremely large values of G or $G \times F$ (in the range of many millions and even billions), these samples were generated using Gaussian statistics extrapolated from smaller batches—in the range of 50,000 to 60,000.

I. ALR Detection With Unknown Frequency and Zero Frequency Drift

The simulation was run for $B = 2000$ Hz, $T = 1000$ s ($G = 2 \times 10^6$), $P_{FA} = 2 \times 10^{-4}$, and $-18.0 \leq P/N_0 \leq 10.0$ dB-Hz. Both the best case (true received frequency falling on one of the bin frequencies) and the worst case (true received frequency falling midway between two bin frequencies) were simulated. The number of trials was set to 60,000. Since we were unable to generate samples for $G = 2 \times 10^6$ or larger, the first and second moments at the output of the summing device were computed using $G = 40$ for both the H_0 and H_1 hypotheses and then extrapolated to $G = 2 \times 10^6$. Figure 6 summarizes simulation results in terms of probability of miss, $P_M = 1 - P_D$, versus P/N_0. The theoretical performance of the MLR scheme is included in this figure for comparison purposes.

The MLR detector with unknown frequency was also simulated, and the results matched almost exactly the theoretical predictions.

II. ALR Detection With Unknown Frequency and Nonzero Frequency Drift

Here the conditions were as in case 1, but with the addition of an extra dimension to compensate frequency drift. This extra dimension had $F = 25,000$ bins. Only the best case (zero frequency offset and zero frequency drift) was simulated. Again extrapolation was used with the Gaussian assumption to generate samples for $G \times F = 5 \times 10^{10}$ bins. Two simulation points at $P_{FA} = 2 \times 10^{-4}$ were obtained at $P/N_0 = -14$ and $P/N_0 = -12$ dB-Hz (each point took 60 hours to compute). These two data points are included in Fig. 6.

The simulation program for the ALR scheme allows for any frequency offset and frequency drift values. However, we did not run a full-scale simulation for $G \times F = 5 \times 10^{10}$ because it would require about 730 years of computation time on a 133-MHz Pentium computer! We feel that even a supercomputer could not handle such a big job. So for the time being, all performance curves for large G and $G \times F$ values are obtained as previously mentioned, by extrapolating to these large values assuming Gaussian statistics.

III. Subband Receiver

The simulation was run assuming $B = 2000$ Hz, $T = 1000$ s, and a subdivision of the total frequency span from 1 to 2000 subbands. Also included was the frequency drift matching case with 50 frequency drift bins covering a ± 25 mHz/s range. Again, probabilities of false alarm and detection were computed by running 60,000 trials for each SNR point in the region of $-12.0 \leq P/N_0 \leq 6.0$ dB-Hz. Figure 9 summarizes these simulation results.

Appendix D

On the Orthogonality of Chirp Signals

In this appendix, we consider the envelope of the correlation function of chirp signals and determine the conditions for their approximate orthogonality.

Consider a received signal of the form

$$r(t) = \sqrt{2P}\cos\left[2\pi\left(f_c t + \frac{1}{2}\dot{f}_c t^2 + \theta\right)\right] + n(t) \tag{D-1}$$

whose signal component is in the form of a chirp signal. To implement the ALR receiver, we must first form the I and Q correlations, $L_c(f, \dot{f}), L_s(f, \dot{f})$, and then form the signal envelope, $L(f, \dot{f})$, all of which are defined in Eq. (43) of the main text. Substituting Eq. (D-1) into Eq. (43) of the main text and ignoring the noise components gives

$$\left.\begin{aligned} L_c\left(f, \dot{f}\right) &= \sqrt{P}C_{cc}\left(\Delta f, \Delta\dot{f}\right)\cos\theta - \sqrt{P}C_{sc}\left(\Delta f, \Delta\dot{f}\right)\sin\theta \\ L_s\left(f, \dot{f}\right) &= \sqrt{P}C_{cs}\left(\Delta f, \Delta\dot{f}\right)\cos\theta - \sqrt{P}C_{ss}\left(\Delta f, \Delta\dot{f}\right)\sin\theta \end{aligned}\right\} \tag{D-2}$$

where (ignoring double harmonic terms)

$$\left.\begin{aligned} C_{cc}\left(\Delta f, \Delta\dot{f}\right) &= \int_0^T \cos\left[2\pi\left(\Delta f t + \frac{1}{2}\Delta\dot{f}t^2\right)\right] dt = C_{ss}\left(\Delta f, \Delta\dot{f}\right) \\ C_{sc}\left(\Delta f, \Delta\dot{f}\right) &= \int_0^T \sin\left[2\pi\left(\Delta f t + \frac{1}{2}\Delta\dot{f}t^2\right)\right] dt = -C_{cs}\left(\Delta f, \Delta\dot{f}\right) \end{aligned}\right\} \tag{D-3}$$

and

$$\left.\begin{aligned} \Delta f &\triangleq f_c - f \\ \Delta\dot{f} &\triangleq \dot{f}_c - \dot{f} \end{aligned}\right\} \tag{D-4}$$

Forming the squared envelope from the I and Q components in Eq. (D-2) gives

$$L^2\left(f, \dot{f}\right) \triangleq L_c^2\left(f, \dot{f}\right) + L_s^2\left(f, \dot{f}\right) = P\left[C_{cc}^2\left(\Delta f, \Delta\dot{f}\right) + C_{sc}^2\left(\Delta f, \Delta\dot{f}\right)\right] \tag{D-5}$$

Using Eqs. (7.4.38) and (7.4.39) of [6], we obtain

$$\begin{aligned} C_{cc}\left(\Delta f, \Delta\dot{f}\right) = T\sqrt{\frac{1}{2\Delta\dot{f}T^2}} \Bigg\{ &\cos\left(\frac{\pi\left(\Delta f T\right)^2}{\Delta\dot{f}T^2}\right)\left[C\left(\sqrt{2\Delta\dot{f}T^2} + \sqrt{\frac{2\left(\Delta f T\right)^2}{\Delta\dot{f}T^2}}\right) - C\left(\sqrt{\frac{2\left(\Delta f T\right)^2}{\Delta\dot{f}T^2}}\right)\right] \\ &+ \sin\left(\frac{\pi\left(\Delta f T\right)^2}{\Delta\dot{f}T^2}\right)\left[S\left(\sqrt{2\Delta\dot{f}T^2} + \sqrt{\frac{2\left(\Delta f T\right)^2}{\Delta\dot{f}T^2}}\right) - S\left(\sqrt{\frac{2\left(\Delta f T\right)^2}{\Delta\dot{f}T^2}}\right)\right]\Bigg\} \end{aligned} \tag{D-6a}$$

and

$$\begin{aligned} C_{sc}\left(\Delta f, \Delta\dot{f}\right) = T\sqrt{\frac{1}{2\Delta\dot{f}T^2}} \Bigg\{ &\cos\left(\frac{\pi\left(\Delta f T\right)^2}{\Delta\dot{f}T^2}\right)\left[S\left(\sqrt{2\Delta\dot{f}T^2} + \sqrt{\frac{2\left(\Delta f T\right)^2}{\Delta\dot{f}T^2}}\right) - S\left(\sqrt{\frac{2\left(\Delta f T\right)^2}{\Delta\dot{f}T^2}}\right)\right] \\ &- \sin\left(\frac{\pi\left(\Delta f T\right)^2}{\Delta\dot{f}T^2}\right)\left[C\left(\sqrt{2\Delta\dot{f}T^2} + \sqrt{\frac{2\left(\Delta f T\right)^2}{\Delta\dot{f}T^2}}\right) - C\left(\sqrt{\frac{2\left(\Delta f T\right)^2}{\Delta\dot{f}T^2}}\right)\right]\Bigg\} \end{aligned} \tag{D-6b}$$

where $C(x)$ and $S(x)$ are the Fresnel integrals defined by [6]

$$\left.\begin{aligned} C(x) &= \int_0^x \cos\left(\frac{\pi}{2}y^2\right) dy \\ S(x) &= \int_0^x \sin\left(\frac{\pi}{2}y^2\right) dy \end{aligned}\right\} \tag{D-7}$$

Substituting Eqs. (D-6a) and (D-6b) into Eq. (D-5) results after simplification in

$$L^2\left(f,\dot{f}\right)=\frac{PT^2}{2}\left(\frac{1}{\Delta\dot{f}T^2}\right)\left\{\left[C\left(\sqrt{2\Delta\dot{f}T^2}+\sqrt{\frac{2\left(\Delta fT\right)^2}{\Delta\dot{f}T^2}}\right)-C\left(\sqrt{\frac{2\left(\Delta fT\right)^2}{\Delta\dot{f}T^2}}\right)\right]^2\right.$$

$$\left.+\left[S\left(\sqrt{2\Delta\dot{f}T^2}+\sqrt{\frac{2\left(\Delta fT\right)^2}{\Delta\dot{f}T^2}}\right)-S\left(\sqrt{\frac{2\left(\Delta fT\right)^2}{\Delta\dot{f}T^2}}\right)\right]^2\right\} \tag{D-8}$$

Noting that $C(0)=S(0)=0$, then for $\Delta f=0$, Eq. (D-8) simplifies to

$$L^2\left(f,\dot{f}\right)\Big|_{\Delta f=0}=\frac{PT^2}{2}\left(\frac{1}{\Delta\dot{f}T^2}\right)\left\{C^2\left(\sqrt{2\Delta\dot{f}T^2}\right)+S^2\left(\sqrt{2\Delta\dot{f}T^2}\right)\right\} \tag{D-9}$$

which, in the further limiting case of $\Delta\dot{f}=0$, gives

$$L^2\left(f,\dot{f}\right)\Big|_{\Delta f=0,\Delta\dot{f}=0}=PT^2 \tag{D-10}$$

in agreement with the results in Eq. (13) of [1]. Further noting that

$$\lim_{x\to\infty}C(x)=\lim_{x\to\infty}S(x)=\frac{1}{2} \tag{D-11}$$

we see that for sufficiently large $\Delta\dot{f}$, the squared envelope of Eq. (D-9) vanishes. The question to be addressed is how large must $\Delta\dot{f}$ be in order for the squared envelope of Eq. (D-9) to approximately vanish, which determines the minimum spacing between quantized values of $\dot{f}$ for approximate orthogonality. Figure D-1 is a plot of $L^2(f,\dot{f})\,|_{\Delta f=0}\,/PT^2$ versus $\sqrt{2\Delta\dot{f}T^2}$, which is in the form of $\left[C^2\left(x\right)+S^2\left(x\right)\right]/x^2$ as obtained from Eq. (D-9). As can be seen from this illustration, the squared envelope is small for $x=\sqrt{2\Delta\dot{f}T^2}\geq 2$. Thus, approximate orthogonality is achieved by spacing the frequency rates an amount equal to $\Delta\dot{f}=2/T^2$, which yields a total number of quantized values in the uncertainty interval $\dot{B}$ of $F=\dot{B}/\left(2/T^2\right)=\dot{B}T^2/2$. Using Eq. (D-8), we see that for $\sqrt{2\Delta\dot{f}T^2}=2$ (the value used for the ALR), the normalized squared envelope (i.e., the correlation coefficient) for $\Delta f=1/T$ and $\Delta f=2/T$ is smaller than its value for $\Delta f=0$ (see Table D-1). Thus, the orthogonality assumption is even more justified.

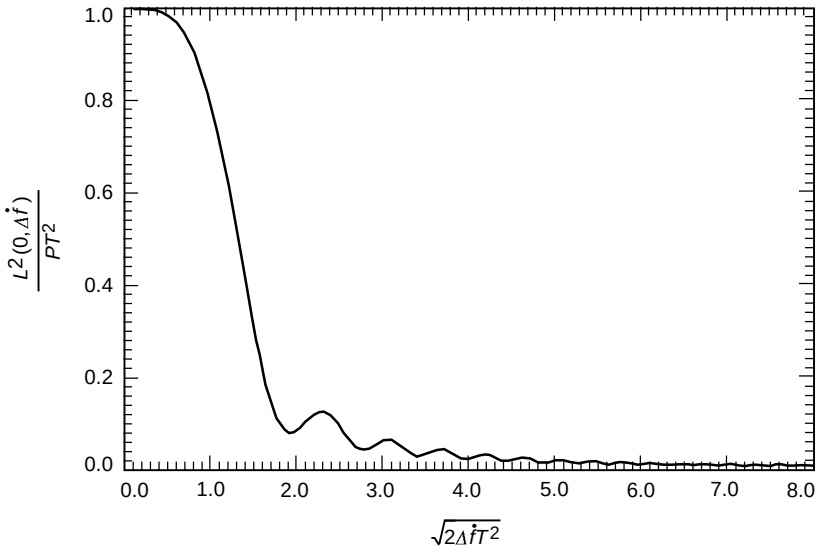

Fig. D-1. A plot of $L^2(f,\dot{f})|_{\Delta f=0}$ / PT^2 versus $\sqrt{2\Delta\dot{f}T^2}$.

Table D-1. Correlation coefficient values for $\sqrt{2\Delta\dot{f}T^2} = 2$ and several values of Δf.

Δf	$L^2 = PT^2$
0	0.089
$1/T$	0.027
$2/T$	0.0015